The Role of SPARC in Aqueous Humor Outflow and TGFß2-mediated Ocular Hypertension in a Murine Model

Abstract

Glaucoma is the leading cause of irreversible blindness worldwide, and is a major cause of blindness in the United States. It affects approximately 5% of Caucasians and 10% of African-Americans over the age of 60 years. Elevated intraocular pressure (IOP) is currently the only modifiable risk factor for glaucoma. Impaired outflow of aqueous humor from the eye is thought to be the cause of pathologically elevated IOP. However, the etiology of outflow impairment is unknown. Anatomically, the aqueous humor drains into the iridocorneal angle of the eye, where the iris inserts at the transition between the cornea and sclera. In humans, approximately 80-90% of the aqueous traverses through the trabecular meshwork (TM), juxtacanalicular connective tissue (JCT), Schlemm's canal, collector channels and empties into episcleral veins. Abnormalities at these sites are thought to cause impaired outflow. Abnormal accumulation of extracellular matrix (ECM) in the TM or JCT, abnormal endothelial function in Schlemm's canal, or a combination of these components have been strongly implicated. Our laboratory has focused on the role of Secreted Protein Acidic and Rich in Cysteine (SPARC) in regulating outflow. SPARC is the prototypical matricellular protein that mediates ECM organization and turnover in numerous human tissues. Our lab was first to demonstrate that SPARC is highly expressed in the TM and JCT regions of the eye, and that the SPARC knockout (KO) mouse has a significant decrease in IOP of 15-20%. SPARC may affect the degree of segmental flow, a theory that states that variable aqueous outflow occurs around the circumference of the eye; only certain portions of the TM are thought to display active outflow at any particular moment.

The cytokine transforming growth factor-ß2 (TGFß2) has been shown to modulate multiple ECM proteins, including SPARC. TGFß2 is significantly upregulated by 2 to 3-fold in the aqueous humor of glaucoma patients compared to controls. In addition, when TGFß2 is overexpressed in rodent eyes, increased ECM deposition is observed within the trabecular

meshwork leading to IOP elevation. SPARC is one of the most highly upregulated proteins by TGFß2, and is downstream of TGFß2.

We hypothesized that wild-type (WT) mice would demonstrate segmental flow, while SPARC KO mice would display a more continuous pattern of outflow around the eye. We also believed that IOP would be inversely correlated with outflow area. We also hypothesized that SPARC is essential to the process of TGFß2-mediated ocular hypertension, and that the lack of SPARC would impair IOP elevation.

We conducted a tracer study utilizing fluorescent microbeads to determine the location of outflow circumferentially around the mouse TM. Microbeads were injected intracamerally into the eyes of WT and KO mice. After a 45-minute incubation period, the mice were euthanized and eyes were processed for confocal, light, and electron microscopy. During the second group of experiments, empty or TGFß2-containing adenovirus was injected intravitreally into WT and SPARC KO mice and IOP was measured for 2 weeks. Immunohistochemistry was completed on all tissues to assess for changes in major ECM proteins.

Percentage effective filtration length (PEFL), or area of the TM labeled by tracer, was significantly increased in SPARC KO mice (70.61% ± 11.36%, $p<0.005$; N=11) compared to WT mice (54.68% ± 9.95%; N=11). In addition, the pressures between the two sets of eyes were significantly different with mean pressures of 16.3 mm Hg in WT mice and 12.6 mm Hg in KO mice ($p<0.005$, N=11 pairs). In addition, PEFL and IOP were inversely correlated with $R^2 = 0.72$ (N=10 pairs); in eyes with higher IOP, PEFL was reduced. Electron microscopy demonstrated that high-tracer TM areas had a greater separation between trabecular beams. Collagen fibril diameter was found to be smaller in the KO (28.272 nm) compared to WT (34.961 nm; $p<0.0005$, N=3 pairs). These data provided structural correlations to the functional data regarding segmental flow.

In the second set of experiments, IOP was found to be significantly elevated in TGFß2-injected WT mice compared to empty vector-injected WT mice during days 4-11 ($p<0.05$, N=8). However, IOP was not significantly elevated in TGFß2-injected KO mice compared to controls. Immunohistochemistry demonstrated that TGFß2 increased expression of collagen IV, fibronectin, plasminogen activator inhibitor-1 (PAI-1), connective tissue growth factor (CTGF), and SPARC within the TM of WT mice, but only PAI-1 and CTGF in KO mice ($p<0.05$, N=3 pairs).

These data support our hypotheses, indicating that SPARC plays an integral role in the modulation of aqueous humor outflow. In addition, it appears as though SPARC is essential to the regulation of TGFß2-mediated ocular hypertension. Aside from providing further evidence of the importance of ECM in IOP regulation, our work presents the novel discovery of segmental flow in the mouse. Given the potential role of SPARC in TGFß2-mediated ocular hypertension, SPARC may not only play an integral role in ECM homeostasis within the trabecular meshwork, but may be a valuable target for pharmacologic therapy in treating primary open-angle glaucoma.

Table of Contents

Glossary

Ad.empty	Sham (empty) adenovirus
Ad.TGFß2	TGFß2-containing adenovirus
ECM	Extracellular matrix
JCT	Juxtacanalicular connective tissue
KO	Knockout
POAG	Primary open-angle glaucoma
SC	Schlemm's canal
SPARC	Secreted Protein Acidic and Rich in Cysteine
TGFß2	Transforming growth factor ß2
TIMP	Tissue inhibitor of metalloproteinase
TM	Trabecular meshwork
WT	Wild-type

Introduction

Glaucoma is a major cause of blindness, affecting over 67 million people worldwide[1]. In the United States, the prevalence is approximately 5% in Caucasians and 10% in African-Americans[2, 3]. While surgical treatments exist, medical therapies have been quite limited due to the lack of insight into the molecular mechanisms behind glaucoma pathogenesis. Elevated intraocular pressure (IOP) is the greatest risk factor contributing to primary open angle glaucoma (POAG)[4], the more prevalent form of glaucoma. Intraocular pressure is determined by the balance of secretion and drainage of aqueous humor, the natural nutrient fluid for the cornea, lens, and trabecular meshwork (TM). Aqueous drains through either the TM or the ciliary body face, both of which are located at the iridocorneal angle where the iris inserts into sclera (Figure 1). The TM extends circumferentially around all 360 degrees of the eye. The proportion of flow between the trabecular meshwork and ciliary body changes with age; in the adult age range of POAG, approximately 80-90% of aqueous humor drains through the TM. After passing through the TM, the fluid traverses through Schlemm's canal (SC), collector channels, and finally empties into episcleral veins (Figure 2). The remaining aqueous humor exits through an alternative pathway, the uveoscleral pathway (Figure 1). While the uveoscleral pathway is manipulated by some glaucoma medications in order to reduce IOP, it is not believed to contribute to outflow dynamics in older eyes[5].

The elevated IOP of POAG is due to impaired outflow through the TM[6]. No defect in aqueous production or drainage through the ciliary body has yet been identified to cause an elevated IOP. The TM is a complex structure of three layers. The two innermost layers consist of endothelial cell-lined supporting beams or fenestrated sheets[6]. The outermost layer, the juxtacanalicular connective tissue (JCT) region, is an amorphous zone of extracellular matrix

(ECM) amongst a small number of cells supported by an incomplete basement membrane, with TM cells on the inner side and cuboidal Schlemm's canal inner wall cells on the outer side[6, 7]. The JCT undergoes constant remodeling. Cells within the JCT are thought to respond to sustained IOP fluctuations by altering the balance of matrix metalloproteinases (MMPs) and tissue inhibitors of metalloproteinases (TIMPs); these alter the quantity and quality of ECM, thereby leading to modulation of outflow resulting in IOP homeostasis[8-10]. One theory is that in glaucomatous eyes, the loss of TM cellularity likely causes an impaired homeostatic response, thereby causing dysfunctional IOP regulation[11, 12]. Consistent remodeling appears to be essential to IOP maintenance.

The role of ECM in outflow regulation and the location of greatest resistance within the iridocorneal angle has been the focus of a great body of literature. Various tissues in the angle are potential sources of resistance: TM, SC, collector channels, and episcleral veins. However, numerous studies have demonstrated that resistance generated within the SC, collector channels, and episcleral veins is minor[13-15]. Earlier studies conducted in the late 1980s demonstrated that in monkeys, a significant portion of IOP reduction occurs slightly upstream of SC, seemingly pointing to the JCT as a key regulatory zone[16, 17]. Further studies demonstrated that the JCT is the anatomic location of the majority (66-76%) of outflow resistance[6, 7]. In today's literature, the synergistic interaction between the JCT, SC endothelium, and the associated fenestrated basement membrane is thought to be the essential component in modulating outflow resistance and IOP[16, 17] (Figure 2). Additional studies comparing normal and glaucomatous human eyes found the greatest difference in JCT morphology; glaucomatous eyes had a significantly thicker JCT region compared to controls[18]. The quick-freeze/deep-etch methodology used to evaluate ECM ultrastructure demonstrated that the JCT contains an intricate mixture of ECM with large open spaces lacking ECM[19]. It is suspected that substances such as proteoglycans and

glycosaminoglycans may account for some of the resistance within the JCT, but this has been challenging to demonstrate using current techniques. SD plaques have been shown to accumulate in this region, which highlight the importance of the JCT in glaucoma pathogenesis[20, 21]; SD plaques are protein aggregates within the TM that correlate with optic nerve damage in glaucomatous human eyes[22]. The JCT region is therefore thought to be a critical component in determining aqueous outflow and potentially in the pathogenesis of glaucoma.

The regulation of aqueous outflow between the JCT and SC endothelium is described by the funneling hypothesis, which states that the aqueous humor funnels through a finite number of pores in the SC endothelium. The funneling process is altered by variation in the distance between the JCT and SC endothelium[23]. Aqueous humor does not exit the anterior chamber of the eye uniformly throughout the 360 degrees of the iridocorneal angle; rather, outflow occurs preferentially at points where there is a more sizeable separation between the JCT and SC endothelium, as well as where there is a higher concentration of pathways leading to episcleral veins[24]. In contrast, flow is reduced in regions where the SC has collapsed, an observation noted in several eyes with high IOP[25]. This concept is referred to as segmental flow. An initial study utilizing cationic ferritin first confirmed the segmental nature of outflow in normal human eyes[26]. In addition, cell-ECM interactions in this region have been found to mediate resistance generation, thereby affecting segmental flow and IOP[8]. Segmental flow has clinical implications in the surgical management of glaucoma. Various TM bypass shunts have been developed in the past few years, such as the iStent[27]. It has been anecdotally discovered that multiple stents are often needed to obtain a substantial decrease in IOP, as one or two devices are often placed in areas of pre-existing high outflow, which does not augment outflow.

Multiple research groups have used microbead tracers to assess segmental flow and have identified an association between IOP and outflow. Zhang *et al*. treated monkeys with argon

laser photocoagulation (a simulation of ocular hypertension in glaucomatous eyes), which led to a 3-fold increase in IOP but a 6-fold decrease in the total TM area utilized for outflow[28]. In addition, the average distance between the two walls of SC was 5-fold lower in laser-treated eyes compared to control eyes, indicating the role of SC collapse in ocular hypertension. The authors concluded that laser damage reduces the available area for outflow, thereby elevating IOP; however, no association data was presented. Similarly, Lu *et al*. showed that WT control eyes demonstrated segmental flow, while eyes treated with the Rho-kinase inhibitor Y-27632 had a more uniform or homogeneous pattern[24]. In addition, treated eyes had a 3-fold increase in the total TM area utilized for outflow, with the JCT and SC wall much more distended. Again, the structural differences in the TM appear to dictate outflow. In the latter study, the authors demonstrated that outflow facility, the reciprocal of resistance to aqueous humor outflow as it leaves the eye, is proportional to the area of TM utilized for outflow. Other groups have utilized fluorescent tracers for anatomic purposes; Lindsey *et al.* and Camelo *et al.* utilized fluorescent dextrans to study aqueous outflow in the rat and mouse[29-33]. The uveoscleral outflow pathway was identified with these techniques in addition to other associated anatomy.

Molecular biology laboratories studying the JCT region have traditionally focused on the TM cells or surrounding ECM. Regarding the former, increase in actin stiffness and the development of cross-linked actin networks (CLANs) have been shown to induce a more rigid morphology in TM cells, leading to decreased outflow[34-36]. Various pharmacologic compounds have been shown to decrease the formation of such stress fibers, leading to increased outflow. These include ethacrynic acid, latrunculins, and Rho-kinase (ROCK) inhibitors[37-42], some of which are currently being evaluated in clinical trials.

Our laboratory investigates the coordinated regulation of ECM in the TM and its effect on IOP. Germaine to this specific work is the role of Secreted Protein Acidic and Rich in Cysteine

(SPARC). SPARC is a matricellular glycoprotein, or a protein that allows cells to communicate with and control their surrounding ECM. Matricellular proteins mediate ECM organization and turnover in various tissues by altering the balance of MMPs and TIMPs, an essential process that occurs within the TM as previously discussed. SPARC is found throughout the human body, and is expressed at a higher level in disease states such as renal fibrosis, hepatic fibrosis, and carcinomas[43, 44]. SPARC has been shown to enhance fibronectin-induced ECM assembly[45], while its removal causes a decrease in the expression of several collagens[46]. SPARC-null mice are prone to several conditions, such as attenuated collagen and connective tissue, poor closure of open wounds, osteopenia, and an impaired reaction against implanted materials[47-50]. SPARC appears to have a strong role in ECM regulation.

In the eye specifically, SPARC can be identified in the aqueous humor and is one of the most highly expressed gene products in the TM[51]. Expression is significantly increased when TM cells are stretched, a physiologic and pathophysiologic consequence of IOP, which may provide additional clues into glaucoma pathogenesis[52]. In addition, SPARC has been implicated in the formation of cataract and corneal repair[53-55]. Various matricellular proteins other than SPARC, such as thrombospondins-1 and 2, hevin, tenascins-C and X, and osteopontin, have been studied in the eye. However, SPARC has a much stronger impact on IOP than any of these proteins[56]. Our lab has demonstrated that SPARC is highly expressed in the human TM[57], and that the SPARC-null mouse demonstrates a significant decrease in IOP of 15-20%[58]. The aqueous drainage pathway in mice is remarkably similar to humans, making it an excellent animal model with findings that are likely applicable to human physiology. We have also demonstrated that when SPARC is overexpressed in perfused human anterior segments, IOP increases by 25-30% with a significant upregulation of fibronectin, collagen I, and collagen IV within the TM[59]. Thus, the mechanism of how SPARC modulates IOP and potentially contributes to glaucoma

pathogenesis warrants further study.

Transforming growth factor ß2 (TGFß2), a critical cytokine in development and tissue growth, has been shown to regulate SPARC and many other ECM proteins in the TM[60-65]. Clinically, TGFß2 is elevated approximately 2 to 3-fold in the aqueous humor of POAG patients [66-69]. *In vitro*, TGFß2 is significantly elevated in cultured glaucomatous TM cell lines compared to normal TM cell lines[70]. In perfused human cadaveric anterior segments, treatment with TGFß2 in the perfusion medium elevates IOP and decreases outflow facility[63, 71]. Additionally, in mouse and rat models, injection of TGFß2-containing adenovirus leads to a significant increase of IOP[64]. The increases in IOP are likely related to changes in ECM, as fibronectin and plasminogen activator inhibitor-1 (PAI-1) are upregulated by TGFß2 in the TM of both perfused cadaveric anterior segments and mouse eyes[64, 65, 71-76]. Thus, TGFß2 and ECM alteration appear to have a critical role in POAG development. TGFß2 appears to regulate SPARC via the Smad 2/3, JNK, and p38 pathways in human TM endothelial cells[77, 78], and SPARC is the most highly upregulated protein in TM cells after TGFß2 stimulation[62]. SPARC may therefore be a critical regulatory node in TGFß2-mediated ocular hypertension.

While there has been substantial progress in our understanding of ECM proteins in glaucoma pathogenesis, the role of specific proteins and pathways are still unclear. Various hypotheses have been postulated, one of which predicts that the amount of ECM in the TM correlates with the amount of outflow resistance, which is supported by intravitreal TGFß2 delivery [8, 79-82]. In addition, the association between the proportion of area utilized for outflow and IOP has not been formally studied. We hypothesized that wild-type mice would exhibit segmental flow, while SPARC knockout mice would display more uniform outflow due to altered ECM production. We also hypothesized that there would be an inverse correlation between the IOP of a mouse eye and the area involved in active outflow. Finally, we

hypothesized that TGFß2-mediated ocular hypertension would be attenuated in the SPARC-null mouse, and that morphologic changes within the iridocorneal angle could be ascertained by immunofluorescence microscopy.

Methods

Animal Husbandry

All experiments were completed in compliance with the Association for Research in Vision and Ophthalmology (ARVO) Statement for the use of Animals in Ophthalmic and Vision Research. Local Institutional Animal Care and Use Committee (IACUC) approval was obtained. C57BL6-SV129 wild type mice and SPARC-null mice with the same background strain were originally obtained by generous donation from E. Helene Sage of the Benaroya Research Institute at Virginia Mason (Seattle, WA). Heterozygotes were bred together, and their offspring were subsequently genotyped in order to identify homozygous SPARC-null mice, which were used in these experiments. In addition, wild-type (WT) and SPARC knockout (KO) breeding pairs were used to increase offspring yield for no more than 1-2 generations in order to limit genetic drift. Animals used in the adenovirus experiments were between 5 and 8 weeks in age. All were housed in the animal biosafety level-2 suite of the Schepens Eye Research Institute animal facility. Animals used in all experiments were housed either in the animal facilities of Massachusetts Eye and Ear Infirmary and Schepens Eye Research Institute.

Passive Binding Assay

To ensure that the affinity for the fluorescent microbead tracer (FluoSpheres carboxylate-modified 20-nm microspheres; Invitrogen, Eugene, OR) utilized in these studies did not differ between the TMs of WT and SPARC-null tissue, WT & KO eyes were passively bathed in a microbead solution. Age and temporally matched WT and KO mice were sacrificed and their freshly enucleated eyes were placed in Dulbecco's Modified Eagle Medium (DMEM) solution. The eyes were then dissected, with the removal of the posterior segment and lens. The anterior

segment was then incubated in a 1:50 solution of microbeads in 1X Dulbecco's Phosphate Buffered Saline (DPBS) -/- (Invitrogen, Eugene, OR) (identical to the injected solution in later studies) for 4 hours in a 37ºC water bath on a shaker, or overnight at 4ºC on a shaker. The tissue was then fixed in Karnovsky's fixative (KII) and sectioned into 6-8 sections. Fluoroscopy of the tissue en face was then completed using an Olympus FSX100 fluorescence microscope (Olympus, Center Valley, PA) with an exposure time of 1/55 second. Images were stitched together using CellSens Imaging Software (Olympus, Center Valley, PA) and fluorescence was quantified using ImageJ software (NIH, Bethesda, MD). Total corrected fluorescence (TCF) was calculated for each section as TCF = integrated density – (area of TM section * mean background fluorescence), akin to calculations in various publications[83, 84]. Mean background fluorescence was averaged from 4 different areas adjacent to the TM. TCF values for the various sections were then averaged to determine the mean TCF value for that eye. Tissue was then analyzed by confocal and electron microscopy.

IOP measurement

Age and temporally matched C57BL6-SV129 wild-type (WT) and SPARC knockout (KO) mice were used. In the segmental flow experiments, each mouse was anesthetized with an intraperitoneal injection of 5 µL/g anesthesia (90 mg/kg ketamine + 9 mg/kg xylazine; Phoenix Pharmaceutica, St. Joseph, MO). A rebound tonometer (TonoLab; Colonial Medical Supply, Franconia, NH) was used to measure the IOP of the right eye six times between 4 and 7 minutes after the anesthetic injection. This time period was selected due to prior studies indicating that the IOP is stable during this time[82, 85, 86]. This was repeated three times, and the mode of each set was calculated and averaged, which was recorded as the IOP for that mouse. The tonometer was fixed horizontally and a pedal was used to initiate measurements to eliminate potential artifact

caused by handling of the device. The probe tip was approximately 2-3 mm from the eye at resting state, and the mouse was positioned to allow the probe to contact the central cornea perpendicularly. The accuracy of the rebound tonometer in measuring IOP has been previously validated in our species of WT and KO mice[58]. All measurements and injection experiments were conducted between 11 AM and 3 PM to minimize the potential artifact from circadian variability on IOP[58].

IOP Measurement under Anesthesia

To demonstrate that IOP remains stable under an inhaled anesthetic, measurements were completed using isoflurane. Age and temporally matched WT and KO mice were used. Each mouse was anesthetized with 2-4% isoflurane (IsoSol; Vedco, St. Joseph, MO) in 1-2 L/min 100% oxygen in a closed chamber; a timer was started when isoflurane was released into the chamber. After precisely 70 seconds, the sedated mouse was moved to a facemask, through which it received 1-1.5% isoflurane mixed with the same concentration of oxygen. IOP was measured every minute between 4 and 15 minutes on either the left or right eye (randomly chosen for each mouse) without adjusting the stand or tonometer as detailed above. IOP was not measured before 4 minutes, as the mouse was not sufficiently anesthetized prior to this time to allow corneal contact. Artificial tears were not administered, as a previous trial demonstrated that it caused aberrations in IOP measurement (data not shown). The cornea appeared to be normal under the current study conditions.

Microbead injection

Mice were then stabilized on a mounting stage (Stoelting Co., Wood Dale, IL) under a zoom-dissecting microscope. The animal was positioned such that the eye was as horizontal as

possible (i.e., iris plane parallel to the stage) in order to ensure even distribution of tracer throughout the anterior chamber. A 10 µl Hamilton microsyringe (Nanofil; World Precision Instruments, Sarasota, FL) was loaded with 1 µL of 1:50 solution of microbead tracer diluted in 1X DPBS -/-, as well as 2 µL of KII solution separated by a 0.1 µL air bubble. Smaller 20-nm microspheres were utilized to ensure that the IOP did not artificially elevate from mechanical blockage from the beads themselves. Multiple rinses with the tracer were completed in order to prevent contamination of the tracer volume in the syringe with KII solution. A 35G needle (NF35BL-2, World Precision Instruments, Sarasota, FL) connected to this syringe was then inserted into the right eye anterior chamber centrally to optimize uniform, intracameral distribution of the tracer. The tracer volume was then delivered at 4 nL/second, by a microprocessor-based microsyringe pump controller (Micro4; World Precision Instruments, Sarasota, FL). Lubricating eye drops (Nature's Tears (hypromellose 0.4%); Rugby Laboratories, Duluth, GA) were applied to the exterior of the eye in order to prevent dehydration. The 12 o'clock position of the eye was marked using tissue marker dye (Triangle Biomedical Sciences, Durham, NC) to provide orientation. At 30 minutes, half of the original dose of anesthesia administered was given in order to maintain the mouse at the appropriate level of sedation.

A time-course experiment was first performed to determine the optimal incubation time for tracer to migrate through the anterior chamber and strongly penetrate the TM and SC. This was found to be 45 minutes, which was then used for all further experiments. The needle remained in the eye during this period, and 2 µL of KII solution was subsequently injected into the anterior chamber of each eye. KII solution was also simultaneously applied to the exterior of the eye multiple times using a plastic dropper. After 30 minutes of fixation, the mouse was sacrificed by anesthetic overdose (4x the original dose), and the eyes were enucleated using a lateral canthotomy technique to reduce trauma to the globe. Eyes were placed in KII solution at

4ºC overnight. If precipitated tracer was observed within the syringe or if the needle made contact with the lens, the experiment was abandoned due to the reduction in effective tracer concentration.

Tissue handling for confocal microscopy

After overnight fixation, each eye was dissected, with the posterior cup and lens removed and the anterior portion partially dissected into 6-8 sections in a "sunflower"-like pattern. The eye was mounted on a slide, with the orientation of the tissue maintained by orienting the tissue with the superior portion placed superiorly on the slide. Sections were viewed en face, and radial and frontal sections were prepared and examined.

Although auto-fluorescence of the iris was noted, this tissue was not removed due to the potential loss or disruption of TM tissue during that process. Fluorescence in the sample was then visualized using a confocal microscope (Carl Zeiss 510 Axiovert M100 Laser Scanning Microscope; Carl Zeiss, Heidelberg, Germany) with a 10X objective and a pinhole of 169 μm in order to capture the entire fluorescence throughout the thickness of the tissue. The tissue was imaged through the corneal side in order to visualize the fluorescent tracer in the TM. Compiling a set of Z-stack images and quantifying the fluorescence confirmed the same intensity and overall pattern as seen with the large pinhole setting. Images of each of the 6-8 sections of the tissue were captured and analyzed using the Zeiss LSM 510 operating software (Carl Zeiss, Heidelberg, Germany).

The tissue was subsequently sectioned in both radial and frontal planes. Sections were stained with 1:1000 TO-PRO-3 (Invitrogen, Eugene, OR) for 30 minutes, followed by three 10-minute washes using 1X DPBS. Radial sections were then evaluated using confocal microscopy

to identify TM and SC, as well as episcleral veins. Frontal sections, orthogonal to radial sections, were then prepared with the guidance of the previously observed fluorescence.

Analysis of Percent Effective Filtration Length (PEFL)

Images were then analyzed to quantify the overall outflow area in the eye. In each section, "total length" of the TM (TL) and "filtration length" of TM containing tracer (FL) were quantified. Percent effective filtration length (PEFL = FL/TL * 100%) was subsequently calculated as performed in previous studies (Figure 3)[24, 28]. Tracer-containing TM was only included in the measurement if the fluorescence created a clear banded pattern and if confocal microscopy confirmed microbead deposition along the JCT and inner wall of Schlemm's canal; irregular, hazy points of fluorescence were not included. If a specific tissue section required two images, a landmark within the tissue was used to prevent measurement overlap. Overall PEFL for the entire eye was calculated by averaging all PEFL measurements. A masked second investigator reviewed the quantification process to ensure its validity (n=10 images). If any disagreement arose, a third party would determine the accuracy of the calculations. The investigators would then review the data points in question together and identify the reason for the discrepancy in order to prevent future disagreements. Statistical analyses comparing PEFL and IOP of WT and SPARC KO mice were completed using a 2-tailed paired Student's t-test. Correlation between PEFL and IOP and the associated coefficient of determination (R^2 value) was calculated using Microsoft Excel. SAS Software (SAS, Cary, NC) was used to run a regression diagnostic; the Studentized Residual Test was utilized to identify any outliers within the linear regression data. An outlier was defined as any residual point with the standard deviation absolute value greater than 3. Prism 5 (GraphPad Software, La Jolla, CA) was used to create all graphs.

Light and Electron Microscopy

Sections containing TM and SC that displayed a high concentration of fluorescent tracer ("high-tracer") or absent tracer ("low-tracer") by confocal microscopy in both WT and KO eyes were then processed for light and electron microscopy. Sections were post-fixed with 2% osmium tetroxide (Electron Microscopy Sciences, Hatfield, PA) in 1.5% potassium ferrocyanide (Fischer Scientific Company, Fair Lawn, New Jersey) for 2h. Sections were then dehydrated using a graded series of ethanol and subsequently embedded in Epon-Araldite mixture (Electron Microscopy Sciences, Hatfield, PA). Semi-thin sections (2 μm) were cut and analyzed using light microscopy with an Olympus BX40 microscope (Olympus, Center Valley, PA). Sections containing regions of interest were then prepared for electron microscopy; thin sections (90 nm) were produced, stained with uranyl acetate (Fischer Scientific Company, Fair Lawn, New Jersey), and examined using transmission electron microscopes (Phillips EM 300, Eindhoven, Netherlands and JEOL JEM-1011, Tokyo, Japan). Images were taken along SC at varying magnifications. Additional details regarding the processing can be found in previous publications[25]. For collagen fibril diameter measurements, EM images at x40,000 magnification were used. A total of 150 fibrils counted from 5 different areas within the JCT were used to compute an average diameter for each subtype (i.e., WT high-tracer, WT low-tracer, etc.). Thus, a total of 300 fibers were counted for each eye. Only fibers that were clearly cut in cross-section were included, in order to ensure accurate measurement of fibril diameter. Image J (NIH, Bethesda, MD) was utilized to measure the collagen fibril diameter. Microsoft Excel was used to perform statistical analyses and Prism 5 (GraphPad Software, La Jolla, CA) was used to create graphs.

Intravitreal Injection

Adenoviruses containing either an empty vector or an hTGFß2 mutant constructs were generated by Allan Shepard (Ad5.CMV.hTGFß2mut & Ad5.CMV.empty)[64]. The hTGFß2 construct was mutated at amino acids 226 and 228 to create constitutively active hTGFß2 in the tissue; additional details on engineering of the adenoviruses have been previously published[64]. The mouse was anesthetized with an intraperitoneal injection of 5µL/g ketamine/xylazine mixture (90mg/kg ketamine + 9mg/kg xylazine; Webster Veterinary Supply, Devens, MA). After reaching a suitable level of anesthesia (confirmed by absence of toe-pinch reflex), the mouse was positioned on a mounting stage (Mouse and Neonatal Rat Adaptor). Using a 10 µl Hamilton microsyringe (Nanofil) connected to a 35G needle (NF35BL-2), empty (hereby referred to as Ad.empty) or TGFß2-containing adenovirus (hereby referred to as Ad.TGFß2) was injected into the intravitreal space of the right eye, just posterior to the limbus, for a final viral titer of 6×10^6 pfu (1.5µL of 4×10^9 pfu). The volume was delivered at 4 nL/s by a microprocessor-based microsyringe pump controller (Micro4). Lubricating eye drops (Nature's Tears; Rugby Laboratories, Duluth, GA) were applied to the cornea to prevent dehydration during the injection. After completion of the injection, the needle was rapidly withdrawn, and the presence of the needle in the desired space was confirmed with observation of vitreous on the needle tip. One drop each of proparacaine 0.5% (Alcaine; Alcon, Fort Worth, TX), ofloxacin 0.3% (Akorn, Lake Forest, IL), and prednisolone acetate 1% (Pacific Pharma, Irvine, CA) was applied to the injected eye to minimize pain, risk of infection, and inflammation respectively, in accordance with IACUC policy. Prednisolone was necessary to prevent the formation of corneal edema; a pilot study demonstrated that without an anti-inflammatory, injection of either Ad.TGFß2 or Ad.empty led to significant corneal edema, thereby confounding IOP measurements using rebound tonometry (data not shown).

Tissue Processing & Histology

After determining the overall IOP trend in a cohort of WT and KO mice injected with TGFß2 over approximately 2 weeks, the peak IOP was noted to be 8 days after injection. A smaller cohort of mice was subsequently injected with Ad.empty and Ad.TGFß2 for morphologic analysis specifically at this time point of 8 days. At that time, the mice were euthanatized with CO_2, and their eyes were enucleated immediately for fixation in 10% formalin (VWR International; Radnor, PA) for 48 hours at room temperature, followed by 70% ethanol at 4ºC. Eyes were then processed and embedded in paraffin wax for serial sectioning of 5µm-thick sections, which were stained with hematoxylin and eosin.

Immunohistochemistry

The following antibodies were utilized in this study: collagen I (600-401-103-0.1; Rockland, Gilbertsville, PA), collagen IV (AB756P; EMD Millipore, Billerica, MA), collagen VI (SAB4500387; Sigma Aldrich, St. Louis, MO), fibronectin (ab23750; Abcam, Cambridge, MA), laminin (AB2034; EMD Millipore), PAI-1 (ab28207; Abcam), connective tissue growth factor (sc-14939; Santa Cruz, Dallas, TX), SPARC (AF942; R&D Systems, Minneapolis, MN), TGFß2 (ab36495; Abcam). Sections were washed with xylene and subsequently hydrated with ethanol dilutions (100%, 95%, 70%.) Tissue was then blocked in 5% bovine serum albumin (when probing for fibronectin) or 10% donkey serum (all other antibodies) for 1 hour at room temperature. Animal serum contained fibronectin epitopes, making it incompatible with the fibronectin antibody. Tissue was then permeabilized using 0.2% Triton-100 and primary antibody was applied at 1:100 concentration overnight at 4ºC. Slides were subsequently washed with 1x PBS-T and 1:200 secondary antibody was applied for 1 hour at room temperature. Slides were washed once again, and the tissue was imaged using the Zeiss Axiovert 200M inverted

fluorescent microscope (Carl Zeiss; Heidelberg, Germany) attached to a digital camera (AxioCam MR3; Carl Zeiss). Images were obtained using the associated software (Axiovision 4.8.2; Carl Zeiss). Slides of tissue treated with Ad.empty and Ad.TGFß2 were imaged at the same time using the same control slide to minimize background.

Fluorescence Intensity Measurements

Quantification of fluorescence was completed using previously established methodology[59, 87-89]. Briefly, the section stained with secondary antibody only was used to identify optimal exposure times for target ECM proteins (Alexa Fluor 488) and TGFß2 (Alexa Fluor 594) that would eliminate signal due to nonspecific binding. These exposure times were used to image fluorescence from target protein and TGFß2 expression in all other sections. Three areas within the TM were selected at random for each section, and ImageJ (NIH, Bethesda, MD) was used to calculate the average fluorescence in the 488 and 594 channels using a rectangular area of interest with consistent dimensions (w0.40 x h1.20 μm).

Immunoblotting

Additional intravitreal injections with Ad.empty or Ad.TGFß2 were completed, and the mice were euthanized 8 days after injection (at the time of peak IOP). Eyes were enucleated and placed in 100μL 1X DMEM. Each globe was dissected, with the anterior segment isolated from the lens and posterior segment. Anterior segments were then placed in 50μL 1X radioimmunoprecipitation assay (RIPA) buffer with protease inhibitors and homogenized. The solution was centrifuged at room temperature for 5 minutes at 12,000 RPM. Supernatant was isolated and equal amounts of total protein were mixed with 2X SDS reducing buffer (125 mM of Tris-HCl, pH 6.8, 4% SDS, 20% glycerol, 0.01% bromophenol blue). Using 8%

polyacrylamide gels, SDS-PAGE followed by immunoblotting were performed as previously described[77].

Statistical Analyses

All data were analyzed in Microsoft Excel (Microsoft, Redmond, WA) or Prism 6 (GraphPad, La Jolla, CA). Two-way ANOVA with multiple comparisons followed by *post hoc* Bonferroni correction were completed to compare the three treatment groups to obtain the adjusted p-value. Percentage of IOP change in WT compared to KO was calculated and assessed for statistical significance using the 2-tailed unpaired Student's t-test. Statistical analyses for immunohistochemistry data were completed using paired Student's t-tests, as each individual group of tissue (i.e., WT Ad.empty, WT Ad.TGFß2, KO Ad.empty, KO Ad.TGFß2) was treated together, but at a separate time from other groups comprising the total sample size. Paired t-tests were used to allow for appropriate comparison.

Chapter I

Results

No Significant Difference in WT & KO Affinity for Microbeads

Mean total corrected fluorescence (TCF) of microbeads binding to the TM in bathed WT & KO eyes did not differ, with WT TCF = 6.05 x 10^9 ± 4.37 x 10^8 and KO TCF = 6.19 x 10^9 ± 3.67 x 10^8 at 37ºC (N=5 pairs, p=0.817; Figure 4A). Tracer was uniformly present in all regions of TM in both WT and KO eyes. The experiment was repeated overnight at 4ºC to assess for any temperature effect, which again confirmed no significant difference in TCF (WT TCF = 9.48 x 10^9 ± 5.78 x 10^8, KO TCF = 9.59 x 10^9 ± 6.85 x 10^8; N=4 pairs, p=0.906.) Confocal microscopy demonstrated that microbeads mostly collected between the superficial beams within the TM in both WT & KO (Figure 4C). Electron microscopy also showed no significant difference in the microbead binding. In both tissues, tracer was observed in large, open spaces between trabecular beams (Figure 5). Tracer was not found within the JCT or SC.

Lower IOPs in SPARC KO Mice

Our results confirmed the lower IOP of SPARC KO mice, with a 22.7% reduction in the IOP of SPARC KO mice compared to that of WT mice. The mean WT IOP was 16.3 ± 2.4 mm Hg, while mean KO IOP was 12.6 ± 2.5 mm Hg ($p<0.005$, N=11 pairs).

Segmental outflow in WT eyes, more continuous outflow in SPARC KO eyes

Segmental flow was identified in both WT and SPARC KO mice, but to a much lesser degree in the latter (Figure 6A & B). WT mice had tracer deposition only in specific regions of the eye; however, there was no consistent pattern present among the WT eyes. The deposition

pattern was much more continuous in KO mice. While outflow appeared almost always on the lateral aspects of the WT eye, outflow was more variable in the superior and inferior portions of the eye. Thus, it was not possible to attribute the outflow pattern to the presence of specific venous structures in certain regions. In contrast to data from the passive binding assay, confocal microscopy of high-tracer regions demonstrated the strong presence of microbeads throughout the TM, extending into the deeper portions of the TM along the inner wall of SC; tracer can also be observed within the canal (Figure 6C & D). When viewed en face, high-tracer regions often demonstrated the presence of microbeads within episcleral veins, reflecting the full penetration of microbeads through the TM, Schlemm's canal, and into the venous system (Figure 6E). In contrast, low-tracer regions demonstrated minimal tracer within the TM; no microbeads were found in SC or episcleral veins.

PEFL Higher in SPARC KO Mice

Using tracer distribution as a representation of outflow distribution around the circumference of the eye, the increase in percentage effective filtration length (PEFL = FL/TL) reflects a significant increase in the area of TM utilized for outflow in the KO eye. PEFL significantly increased in SPARC KO mice (70.61% ± 11.36%, N=11) compared to WT mice (54.68% ± 9.95%, N=11, $p<0.005$; Figure 7). Thus, it appears as though the absence of SPARC significantly affects the aqueous humor outflow pattern. A sample confocal microscopy image as well as an estimation of FL and TL, which allows for calculation of PEFL, can be reviewed (Figure 3). In Figure 3A, the tracer is present in the TM overlaying the SC. Figure 3B is an en face view that illustrates how the total length of the TM in this section and the length covered by tracer were quantified.

IOP and PEFL are Inversely Correlated

A negative correlation between IOP and PEFL was observed (Figure 8); PEFL decreased as IOP increased. This suggests that a decrease in the area of bead deposition corresponded to an overall decrease of outflow, linked to a relatively elevated IOP. Conversely, greater bead deposition represented increased outflow of aqueous humor, which was associated with decreased IOP. When fit with a corresponding linear regression line, an R^2 value of 0.59 was calculated (N=22). However, one data point was identified as an outlier by the Studentized Residual Test with a standard deviation of -3.82. When this point and its matched pair were removed from the analysis, R^2 increased to 0.72 (N=20, $p<0.0001$), indicating a more robust association between PEFL and IOP.

High-tracer regions display less compact morphology than low-tracer regions

Electron microscopy images at lower magnification (x8,000) of high-tracer and low-tracer regions in WT and KO eyes demonstrated that high-tracer regions have less compact morphology (N=3 pairs; Figure 9). The JCT and TM in low-tracer images appear to be much more compact, with the trabecular beams layered closer together. In contrast, increased space between trabecular beams was noted in high-tracer samples. The difference in morphologic data is consistent with previous findings in other animal species[24, 28].

Collagen fibril diameter is significantly decreased in JCT of SPARC KO mice

No significant differences in morphology were detected between the TM of WT and KO tissues at the light microscopy level (data not shown), consistent with our previously published report[58]; the iridocorneal angles were indistinguishable with the same level of cellularity and sizes of various structures. At higher magnification electron microscopy (x40,000), collagen

fibril diameter within the JCT was found to be significantly decreased in SPARC KO mice (28.272 nm) compared to WT mice (34.961 nm, $p<0.0005$, N=3 pairs; Figure 10). If differentiated into high-tracer vs. low-tracer regions of WT & KO tissue, collagen fibril diameter was significantly decreased in both high-tracer regions of KO tissue compared to that of WT (27.232 nm and 35.459 nm respectively, $p<0.0005$) and in low-tracer regions of KO vs. WT (29.312 nm and 34.462 nm respectively, $p<0.0005$).

Microbeads were also found in the open spaces of the JCT in high-tracer regions at this higher magnification (Figure 11). Microbeads were not identifiable in the JCT of low-tracer regions, a consistent finding given its more compact extracellular matrix (Figure 9). More tracer was also found in the JCT regions facing the collector channel ostia, beneath the gaps amongst inner wall endothelial cells.

Discussion

Our results contribute new data to the field while confirming previous results. This study was novel in discovering the presence of segmental flow in the mouse species, which had not been previously demonstrated. This finding is unique also because of its evolutionary implication. Since segmental outflow has been observed in the human, monkey, bovine eyes, and now the distant rodent of the mouse, the segmental pattern of outflow may be strongly conserved amongst mammalian species. This is the first observation of segmental flow in a small mammal. We were unable to assess a potentially dynamic nature to flow patterns (i.e., changes from high-tracer to low-tracer states) due to our inability to assess outflow in each eye more than once. It is possible that changes could occur due to alterations in positioning of the eye. The impact of gravity on outflow should be considered here as well.

Our results also demonstrate a significant increase in PEFL in SPARC KO mice, with an overall change from segmental to more continuous outflow. These results were reproducible in the large sample size that was utilized. With these data corroborating our lab's previous findings regarding the significant decrease in IOP of the KO mouse, this study confirms the influence of SPARC on outflow and creates the basis for a relationship between ECM, filtration area, and IOP. The association between the PEFL and IOP was reasonably strong with an R^2 value of 0.59, even in the presence of an outlier. When this point was removed, the R^2 value increased to 0.72, reflecting a strong correlation. With the increase in PEFL of KO eyes and this association, SPARC appears to be an important modulator of aqueous humor outflow and IOP in mice. In the absence of SPARC, IOP decreases and PEFL increases significantly due to increased outflow observed throughout the entire TM. While correlation does not imply causation, we would still postulate that the lack of SPARC leads to the increase in PEFL, and this increase in overall

outflow is what causes the reduction in IOP. The observed increase in PEFL could be due to a fundamental difference in the ECM composition caused by the lack of SPARC. Again, this is a suggestion based on the results of this study; further investigation is warranted in order to establish this causal relationship. For example, studying any association between SPARC and collagen IV or fibronectin may be of value in investigating how SPARC directly impacts ECM levels. Collagen IV would be of particular interest due to the presence of a basement membrane between the JCT region and Schlemm's canal, which may impact outflow resistance. The validity of such a relationship appears to be greater due to the results of these experiments.

The electron microscopy images that were obtained provide valuable insight into the structural basis of the observed segmental outflow. Light microscopy in this study and a previous publication demonstrated that there were no gross differences between WT and SPARC KO eyes that might influence outflow pathways (e.g., globe size, lens size, iris thickness, or iridocorneal angle degree)[58]. However, utilizing electron microscopy, differences in tracer distribution could be attributed to the compactness of the TM; the less compact the tissue, the greater the outflow of aqueous humor, and the greater the amount of tracer in this region. In contrast, the compact TM inhibited outflow, leading to a minimal amount of tracer in these areas. These structural data corroborate the concept of segmental flow; aqueous humor tends to leave the eye in specific areas depending on the compactness of the TM.

The significant difference in collagen fibril diameter within the JCT of WT & KO tissues reflects the role of SPARC in ECM processing. Significant changes in collagen fibril diameter in other tissues of SPARC-null mice have been reported in previous studies[47, 48]. Bradshaw *et al.* showed that dermal collagen fibrils in SPARC KO mice were significantly smaller and more uniform compared to that of WT mice. They also demonstrated that SPARC was essential to the

maturation of collagen fibers in the dermis, highlighting the effect of SPARC on collagen processing and ECM composition.

In the trabecular meshwork, our data suggests a potential mechanism by which IOP is reduced in SPARC KO mice. With a significant change in collagen fibril diameter, more of the TM is converted into a high-tracer (i.e., less compact) state, which increases outflow as reflected by the PEFL data in this study. This subsequently leads to a decrease in IOP. In contrast, the glaucomatous eye may present increased SPARC expression, reversing these values and leading to increased IOP. Again, we should emphasize that this is a postulated hypothesis of how SPARC may be involved in glaucoma. In addition, the precise relationship between collagen fibril diameter and IOP is unclear. Our group previously reported a decrease in IOP but increased JCT collagen fibril diameter in thrombospondin-1 and 2 (TSP1 & 2) knockout mice[90]. It seems as though the deletion of matricellular proteins affects post-translational processing of collagens[91]. Fibril diameter is regulated by various processes such as crosslinking alteration by crosslinking enzymes (lysyl oxidase, tenascin-X, perlecan) and small leucine-rich proteoglycans (decorin, biglycan, fibromodulin), cleavage of procollagen by proteinases, organization of fibril assembly by fibronectin and integrins, and nucleation by collagen V and XI[92, 93]. SPARC may be involved in modulating one or more of these processes.

It is also possible that SPARC affects the quality of the ECM in the TM, and not necessarily the ultrastructural anatomy. Previous studies have indicated that it is not just the quantity of the ECM, which would be appreciated through electron microscopy, but the quality of the ECM that dictates outflow[94]. In addition, it is possible that the lack of SPARC leads to a decreased amount of compact TM, thereby leading to greater PEFL. The difference may not lie in the morphology itself, but rather how much of the entire TM is densely compact. Additional

studies analyzing the entire TM tissue of a WT and KO mouse eye would be necessary to verify this theory, as evaluating a few samples slides would not provide sufficient data.

Our quantification of PEFL in this experimental model system confers two significant advantages. First, the animal model used was genetically manipulated, leading to an endogenous change in physiologic outflow. This is in contrast to other current models, which often involve enucleated, live eyes or eyes that have artificially impaired outflow induced by laser trauma. Second, this model takes advantage of *in vivo* outflow mechanisms in the mouse to study the spread of the fluorescent tracer. The natural flow of the aqueous humor itself leads to distribution of the tracer rather than artificial perfusion; the mouse eye is still producing aqueous humor during the experiment and pressure gradients are still maintained. Again, this is in contrast to previously published studies, in which live human eyes are perfused at a controlled rate.

Naturally there are certain limitations to this study, which we attempted to minimize as much as possible. One potential issue was artifact in tracer distribution due to gravity. During the experiments, the mouse eye was positioned as horizontally as possible (i.e., plane of the iris was parallel to the table). Other limitations include the inability to monitor IOP during the injection using a probe placed into the anterior chamber through a second insertion site. This was not possible due to the small size of the mouse eye; however, we attempted to minimize an IOP spike by using a slow infusion rate. Another potential concern was a large increase in IOP during the injection experiments, leading to artifact or tissue damage. An injection rate of 4 nL/s was chosen based on similar rates utilized in established studies evaluating fluorescent tracer distribution[29, 30]. However, a transient elevation of IOP may have occurred during the injection phase, given the injection rate was slightly elevated in comparison to the endogenous aqueous humor formation rate (0.14–0.18 μL/min)[95, 96]. Any such IOP elevation could have affected

tracer distribution. Given a potential difference in outflow facility between WT and SPARC-null eyes[58], the magnitude of IOP elevation might have differed between the two strains. Thus, the contrast in tracer distribution between WT and SPARC-null eyes could have been influenced by this potential difference in outflow facility, in addition to baseline IOP. We were unable to separate these factors given our experimental design. However, the differences in tracer distribution are still due to inherent differences between WT and SPARC-null eyes. We also were only able to inject the right eye of each mouse due to constraints of the experimental setup. However, we have no reason to suspect that outflow pathways would differ between right and left eyes. In addition, the right eye was consistently used in both WT and KO mice.

Another concern raised was regarding the use of rebound tonometry for IOP measurement. Since SPARC influences ECM production, one could argue that the biomechanical properties of the cornea could have been affected, leading to abnormal rebound tonometer readings. This criticism has been addressed in a previous publication[58], in which rebound tonometer readings in SPARC KO mice were validated across a wide range of IOPs using direct manometry, which is not sensitive to corneal biomechanics. Furthermore, central corneal thickness (CCT), which could be potentially affected by the lack of SPARC, can affect rebound tonometry measurements. However, Haddadin *et al*. again demonstrated that no significant difference existed between the CCT of SPARC KO and WT mice, thereby eliminating this issue as a confounder in IOP measurements[58]. One study demonstrated that there was near perfect agreement between TonoLab rebound tonometry and manometry in both wild-type and glaucoma model mice[97]. This methodology has gained wide acceptance in the glaucoma research community.

As mentioned above, certain techniques utilized were challenging due to the precise positioning of the needle required within the anterior chamber. The needle could not make contact with the lens or iris, as this would cause abnormal distribution of the tracer; the microbeads could settle within a nick in the lens, thereby reducing the effective tracer concentration reaching the TM. Similarly, damaging the iris would have created an artificial pathway for the microbeads to exit the anterior chamber.

The injection technique had to be altered several times in order to surmount multiple technical challenges. First was determining the route of tracer injection. An intracameral injection allowed for even distribution of the tracer, while an intravitreal injection would not ensure consistent distribution of tracer into the aqueous humor between experiments. Since an even distribution throughout the TM was critical to this study, intracameral injection was chosen. However, leakage from this injection had to be minimized, leading to the exploration of various techniques. A 35G metal needle and a 100-μm silanized glass needle were used in experiments in order to compare the amount of leakage observed. There had been anecdotal reports that leakage would be further reduced with the glass needle due to silanization. However, significant leakage was observed with both methodologies. We decided to utilize the metal needle due to the technical ease. We subsequently needed to decide whether to keep the needle in the eye after the injection was complete and the incubation period had begun. Since significant leakage was observed upon retraction of the needle, the idea of keeping the needle in the anterior chamber for the entire incubation period was explored. Since this would involve exposing the eye to the air for an extended period of time, lubricating drops were applied.

The next obstacle encountered was abnormal morphology of the TM due to retrograde flow of blood from the episcleral veins into SC. This occurred when the needle was removed

after the incubation period. The reflux flow led to dilation of SC and compression of the TM in some eyes, thereby precluding any useful morphologic analyses. The injection protocol was initially altered by loading the syringe with tracer and KII fixative separated by mineral oil. However, this technique failed due to the miscibility of these compounds. We then decided to separate the microbead tracer and fixative with a miniscule air bubble. After consulting multiple experts, it was determined that the injection time was a relatively short period of time, insufficient to cause any oxidative damage to the tissue that might confound the microscopy work. This technique was successfully utilized in maintaining TM anatomy.

The lateral canthotomy method was used instead of traditional methods during enucleation, as no direct pressure was placed on the globe, which could potentially disturb TM morphology or tracer distribution. One unavoidable, potential source of artifact was the pressure applied to the eyeball when inserting the needle into the anterior chamber. Forceps are used to grasp the eyeball during insertion in order to stabilize the eye, which might have increased external pressure thereby affecting TM and SC morphology. However, this step was unavoidable, as the eye had to be immobilized to introduce the needle into the anterior chamber. Both groups were equally exposed to this initial pressure.

The overall fragility of the mouse eye in comparison to that of other species may have contributed to the difficulties encountered with TM morphology as well. The TM was often destroyed while removing the iris during initial experiments. The iris was no longer removed after this was discovered. We also found that the iris auto-fluoresced at the same wavelength of the tracer, leading to some image artifact. However, the unique pattern of tracer within the TM was quickly recognized, which eased our ability to identify and disregard artifact from the iris.

The microbead injection technique has been validated and utilized by various other groups[24, 28]. As previously discussed, Zhang *et al.* and Lu *et al.* used similar tracer microbeads in their studies with monkey and bovine eyes respectively, validating the use of the microsphere technique in studying outflow and outflow resistance. In these studies as well as our work, the microbeads remained in the TM and SC, instead of being washed out, at the time of evaluation. A time-scale experiment was initially conducted in order to determine the optimal incubation time, which was discovered to be 45 minutes; any less time led to the lack of significant tracer in the TM, while additional time led to the tracer being washed out into the episcleral veins. Thus, with this careful determination of the incubation time, we believe that our tracer data is not a washout phenomenon, but rather is a binding phenomenon and is reflective of the true outflow pattern.

Chapter II

Results

IOP Stable Under Isoflurane Anesthesia

Under isoflurane anesthesia, IOP measurements were consistent and stable between minutes 5 and 8 (Figure 12). The difference of IOP between WT and SPARC KO mice was reproducible at all time points ($p<0.05$ at all points; N=8). Mean WT IOP during minutes 5 to 8 was 16.5 ± 2.5 mmHg, while mean KO IOP was 12.4 ± 1.1 mmHg ($p=0.0057$). The mean percentage IOP decrease in KO eyes was 24.6 ± 0.7%.

Immunoblotting Confirmation of TGFß2 infection

Infection of the TM by TGFß2 was verified with immunoblotting (Figure 13). TGFß2 was significantly increased in both WT and KO eyes treated with Ad.TGFß2 compared to eyes treated with Ad.empty (N=4/group, $p=0.0023$ and $p=0.0141$ respectively). There was no significant difference in TGFß2 expression levels between WT and KO Ad.empty-injected eyes ($p=0.7293$). SPARC was also noted to increase significantly in WT tissue by 56.2% with Ad.TGFß2 infection ($p=0.0425$).

IOP Elevation with TGFß2 in WT mice but not SPARC KO mice

In WT mice, a significant difference in IOPs between the Ad.TGFß2-injected and Ad.empty-injected eyes, and between the Ad.TGFß2-injected and uninjected contralateral eyes was detected ($p<0.0001$) (Figure 14). Ad.TGFß2-injected WT mice had an increase of IOP at the fourth day after injection (Day 4), Day 6, Day 8, and Day 11 when compared to the Ad.empty-injected WT mice ($p=0.0166$, 0.0230, <0.0001, 0.0230 respectively; Figure 14). When compared

to the IOPs of uninjected contralateral eyes, Ad.TGFß2-injected eyes had a significant increase during the same period, but the Ad.empty-injected WT eyes had no significant increase compared to uninjected contralateral eyes (Table 1).

A difference in IOP was also observed amongst the treatment groups in KO mice ($p=0.0023$). However, in contrast to WT mice, Ad.TGFß2-injected KO mice had a mild elevation in IOP that was not significant compared to Ad.empty-injected KO mice (Figure 14 & Table 1). If Ad.TGFß2-injected KO eyes were compared to uninjected contralateral eyes, the change in IOP became statistically significant only at Day 8 ($p=0.0385$).

The peak of IOP increase was noted to be at Day 8 for both WT and KO eyes. At this time, the average IOP of Ad.empty-injected WT IOP was 14.3 mmHg, Ad.TGFß2-injected WT IOP 18.3 mmHg ($p<0.0001$), Ad.empty-injected SPARC-null IOP 12.1 mmHg, and Ad.TGFß2-injected SPARC-null IOP 13.0 mmHg ($p=0.7518$).

The difference in percentage of IOP increase between WT and SPARC-null eyes was significant at Days 4, 6, and 8. At Day 8, the percentage increase of IOP from baseline was 28.5 ± 4.2% in WT mice and 14.4 ± 4.9% in KO mice ($p=0.0444$, N=8; Figure 15).

No Change in Angle Morphology

No significant difference was observed between all 4 experimental groups on light microscopy (Figure 16). In contrast to previous findings regarding TGFß2 injection in mice[64], the iridocorneal angle remained open in all groups. No synechiae were observed in the anterior chamber.

Confirmation of TGFß2 infection

Immunohistochemistry was performed on whole eyes to demonstrate tissues infected by Ad.TGFß2. Injected mice were sacrificed at peak IOP, 8 days after adenoviral injection. WT and KO eyes that were uninjected, injected with Ad.empty, or injected with Ad.TGFß2 were sectioned and stained for TGFß2 (Figure 17). TGFß2 staining was similar between uninjected and Ad.empty-injected eyes in both WT and KO tissue. Staining was strongly increased in Ad.TGFß2-injected eyes on Day 8, specifically in the retina, vitreous humor, and trabecular meshwork. Additional Ad.TGFß2-injected mice were sacrificed on Day 13 and their eyes were stained for TGFß2 to demonstrate a reduction in TGFß2 expression to levels similar to Ad.empty-injected eyes.

IHC demonstrates importance of Collagen IV and Fibronectin

Upon TGFß2 stimulation in WT mice, the fluorescence intensity collagen IV, fibronectin, PAI-1, connective tissue growth factor (CTGF), and SPARC were noted to significantly increase 8 days after injection compared to WT mice injected with Ad.empty ($p<0.05$, N=3; Figures 18-20). Collagen I and laminin intensities were also noted to increase, but were not significant. No change was noted in collagen VI levels. When assessing the fluorescence of the same proteins in KO mice 8 days after injection, only the intensities of PAI-1 and CTGF significantly increased with injection of Ad.TGFß2 vs. Ad.empty ($p<0.05$, N=3; Figures 18-20). The collagen IV and fibronectin increase observed in WT mice was attenuated in KO mice and did not achieve statistical significance (Table 2).

Discussion

Based on our intravitreal injection data, SPARC appears to have a key role in TGFß2-mediated ocular hypertension. When compared to eyes injected with Ad.empty, Ad.TGFß2-injected KO eyes demonstrated no significant elevation in IOP. In contrast, the IOP of WT eyes injected with Ad.TGFß2 increased significantly. When compared to the contralateral uninjected eyes, Ad.TGFß2-injected KO mice have a substantial delay of IOP elevation (significant at only one time point, Day 8), a blunting of the magnitude of increase, and shortening of the increase to only one time point. The failure to completely inhibit the IOP response in Ad.TGFß2-injected KO mice likely represents redundancy amongst matricellular proteins. SPARC, thrombospondins-1 and -2, tenascins-C and -X, hevin, and osteopontin have all been shown to have important roles in affecting ECM assembly, MMP activation, and collagen fibrillogenesis[56, 90, 98]. In addition, TGFß2 is also thought to act through other pathways, such as inducing TM cell senescence or altering the actin cytoskeleton[78, 99, 100]. It is likely that these pathways are still active with TGFß2 injection in the SPARC KO mouse.

Our results seem to confirm the previously reported increase in PAI-1 and fibronectin in Ad.TGFß2-injected mice[64]. We also observed an increase of CTGF and collagen IV fluorescence. Shepard *et al*. found an increase, albeit non-significant, in the mRNA levels of these proteins. However, mRNA levels do not necessarily correlate with protein expression, as changes in protein levels could result from mechanisms other than an increase in transcription and translation, such as decreased turnover. We have previously observed this phenomenon with SPARC-induced changes in JCT ECM[59]. Increases of PAI-1 and CTGF, which have been observed in perfused human anterior segments[71], appear to be mediated by mechanisms other than SPARC. CTGF and PAI-1 are often regulated in a similar fashion; both have been shown to

increase in TM cells after TGFß2 stimulation[62, 101]. The elevated levels of PAI-1 in POAG patients and its function in decreasing ECM turnover by inhibiting MMPs underscores the role of ECM dysregulation in glaucoma pathogenesis[102, 103].

Both immunohistochemistry and immunoblot demonstrated an increase of SPARC following TGFß2 stimulation[77]. As previously discussed, SPARC overexpression increased collagen IV and fibronectin within the JCT TM in perfused human anterior segments[59], illustrating conservation of function between humans and mice. TGFß2 overexpression in mice caused increases in collagen I and laminin that did not reach statistical significance, which was also observed in perfused human anterior segments[59]. However, it appears as though some effects are species-specific, as collagen VI was noted to increase with SPARC overexpression in human tissue, but not in TGFß2-stimulated mice.

Collagen IV and fibronectin are significant components of the JCT basal laminae. SPARC stimulates the partial unfolding of fibronectin, which is crucial to overall ECM assembly[45, 104], and is essential to collagen IV deposition[105, 106]. Thus, the deletion of SPARC would be expected to impact basal lamina homeostasis. It is possible that without SPARC, the attenuation of the collagen IV and fibronectin upregulation is significant enough to reduce outflow resistance, and blunt the TGFß2-mediated IOP increase. In addition, we have previously shown that in perfused human anterior segments, SPARC overexpression decreases MMP-9 activity, thereby attenuating ECM degradation[59]. We could surmise that SPARC moderates MMP activity, and that MMP activity is higher in the SPARC-null mouse, leading to greater ECM degradation and a diminished IOP increase. While CTGF and PAI-1 have been shown to be important contributors to ECM synthesis and degradation respectively, they have not been shown to interact with SPARC. The lack of change in their levels in TGFß2-injected SPARC-

null mice seems to suggest that they may work through SPARC-independent pathways to modulate ECM protein expression and MMP activity. We also demonstrated that IOP remains stable in mice between minutes 5 and 8. To our knowledge, this is the first time-course study corroborating the stability of IOP measurements with an inhaled anesthetic in mice; a similar study was conducted in Brown Norway rats[107]. We chose the 5 to 8-minute period because it was early enough to ensure corneal dehydration would not become an active issue and the earliest point at which IOP reached a stable plateau. These data serve as an important confirmation of technique, given the increased utilization of the mouse model in aqueous outflow studies involving IOP measurement.

We also confirmed that a significant IOP decrease in SPARC KO mice compared to that of WT mice was reproducible under isoflurane anesthesia. Our group previously reported a 15-20% IOP decrease in KO mice anesthetized with ketamine/xylazine[58]. Given that inhaled anesthetics are generally known to reduce IOP[107-109], an absolute decrease in IOP values with isoflurane compared to those obtained with ketamine would be expected and was observed. The greater decrease in percentage of baseline IOP (approximately 24%) may simply be normal variability, as we previously found a 22.7% IOP decrease in SPARC KO mice as detailed in Chapter I of this work and elsewhere[110]. Conversely, this percentage change could also be related to the difference in metabolism of isoflurane and ketamine. While ketamine is metabolized by CYP3A4 in the liver[111], isoflurane undergoes minimal hepatic metabolism and is primarily cleared by respiration[112, 113]. Given the known role of SPARC in both ECM assembly and dissolution in the lung[114, 115], it is possible that SPARC KO mice are unable to clear the compound as easily as WT mice, thereby leading to a higher serum concentration and additional impact on IOP.

There were multiple challenges encountered during these experiments. It should be noted that aside from probing for SPARC, immunohistochemistry findings were not corroborated with other forms of molecular analysis due to the difficulty of observing subtle changes in ECM protein expression specifically within the mouse TM. Isolation of mouse TM from cornea and iris is quite challenging, as the TM is fragile and often detaches with the iris or cornea. Invariably, there is contamination by adjacent tissues such as the iris and choroid. We believe that the elevation in SPARC detected by immunoblot of anterior segments was possible due to SPARC being the most highly upregulated protein with TGFß2 stimulation[62]. Other ECM proteins are not nearly as highly upregulated as SPARC, making any increase in expression within the TM difficult to observe by molecular analyses.

There were differences in both methodology and results with TGFß2 overexpression compared to a previous study[64]. First, we used a lower viral titer of 6×10^6 pfu instead of 6×10^7 pfu. In initial studies, a higher titer caused corneal edema as early as one day after injection that could not be prevented with steroid treatment and led to significant artifact when measuring IOP with rebound tonometry. This was a significant challenge in this study; multiple studies were completed using different viral titers with and without topical prednisolone to identify the optimal titer that would induce IOP elevation without corneal inflammation. We also considered resynthesizing the adenoviral vector in order to ensure there were no other confounding causes of the edema (e.g., degradation products inciting an inflammatory reaction). We ultimately found that 6×10^6 pfu was the highest viral titer that led to IOP elevation without corneal edema when one drop of prednisolone was applied after injection. It is unlikely that the IOP elevations observed in our study were a corticosteroid-mediated response from the single topically applied drop containing approximately 30 μg of prednisolone acetate. Even assuming intraocular

penetration of 100% of the available drug contained within a 30 μL drop. In humans, the tear film and conjunctival cul-de-sac can only hold approximately 30 microliters from a topically applied drop[116]. Although the equivalent volumes are unknown in a mouse, it can be safely assumed to be much smaller given the difference in globe size between humans and mice. Corticosteroids require chronic treatment to raise IOP[117]. In mice, there is only a minimal change in IOP even with a subconjunctival dose of 800 μg of triamcinolone[118]. In addition, our lab previously demonstrated that topical prednisolone acetate applied four times daily to the mouse eye does not induce an IOP increase even after 3 weeks (unpublished data).

The difference in mouse strain and age may explain the lower magnitude of IOP increase in our Ad.TGFß2-injected mice, the mild variation of IOP observed in uninjected eyes, and the shorter duration of IOP elevation compared to Shepard *et al*[64]. The duration of IOP elevation was limited, consistent with the natural decay of foreign genetic material within a mammalian cell of 5-12 days[119, 120]. Adenoviral-delivered plasmids remain for approximately 14 days in murine eye tissue[121, 122]. However, other studies have demonstrated that adenovirus can last up to 4 weeks[64, 123-125]. Animals used in those studies were often older and of different strains, and viral titers were higher; we might have observed a more sustained response if a higher viral titer had been used. Immunohistochemistry completed in our study showed that TGFß2 synthesis was attenuated at Day 13 (Figure 17), corroborating our IOP data and illustrating the time course of infection using this particular viral titer in this mouse species. In contrast to the work of Shepard *et al*., our Ad.TGFß2-injected eyes did not display angle closure, which would elevate IOP[64]. The slightly lower viral titer and one-time application of prednisolone could have mitigated the formation of synechiae and subsequent angle closure. Even empty adenovirus has been shown to cause a modest anterior chamber inflammation[64]; the prednisolone may have sufficiently reduced such inflammation to prevent angle closure.

Conclusions and Suggestions for Future Work

This work provides strong evidence implicating SPARC in the regulation of IOP and aqueous humor outflow, further defining the potential role of this protein in glaucoma pathogenesis. Our work demonstrates for the first time that segmental flow exists in the mouse, which was previously unclear amongst the glaucoma TM community. This finding may reflect the importance of segmental flow in mammalian homeostasis, given its strong conservation from the mouse to the human. In addition, this study is novel in its methodology, utilizing an *in vivo* injection system to examine one specific endogenous protein and its effect on outflow and IOP. Due to the role of SPARC in ECM synthesis and degradation, our data provides even further support to the theory that ECM within the TM influences the degree of outflow resistance (i.e., a reduced amount of ECM is equated with reduced outflow resistance). In addition, an inverse correlation between outflow and IOP was identified. The electron microscopy data provides structure-function correlation, indicating that the compactness of the TM tissue affects the degree of outflow, and that SPARC appears to affect collagen fibrillogenesis. By implicating SPARC, our data associates three essential components in glaucoma pathogenesis – the molecular state of the ECM in the TM, the hydrodynamic process of outflow, and the clinical measurement of IOP.

We have also demonstrated that SPARC is essential to modulating TGFß2-mediated ocular hypertension in mice, given the minimal redundancy with other matricellular proteins as demonstrated by this study. This finding is consistent with SPARC being the most upregulated protein with TGFß2 stimulation[62]. Immunohistochemistry suggests that collagen IV and fibronectin levels, which appear to be SPARC-dependent, are vital to the TGFß2-mediated IOP increase. Given our knowledge of the synergistic role of the SC fenestrated basement membrane in outflow resistance, it is unsurprising that these specific proteins are involved. Since TGFß2

has been strongly implicated in the pathogenesis of POAG, SPARC itself may play a role in glaucoma pathogenesis; it may serve as a critical node in this process, mediated by various intracellular pathways previously described. We have also shown that IOP can be accurately and consistently measured in mice with rebound tonometry under isoflurane, a commonly used anesthetic in glaucoma mice models.

Future work includes evaluating whether the outflow-IOP association can be shown to be a causal relationship. Additionally, conducting molecular analyses to understand the mechanisms by which the TGFß2-mediated ocular hypertensive phenotype is inhibited in the SPARC-null mouse would be valuable. Attempting to determine how SPARC mediates ECM levels from a mechanistic perspective (e.g., via integrin activation, binding to MMPs or TIMPs) would be helpful while studying how SPARC may be involved in glaucoma pathogenesis. From an engineering perspective, it would be highly valuable to the field to identify a technique that would allow *in vivo* visualization of segmental flow; this could have significant implications in the research community as well as in clinical practice. Finally, attempting to inhibit SPARC through small molecule inhibitors or viral vectors would provide insight into SPARC as a potential therapeutic target.

Summary

Glaucoma is a painless eye disease affecting millions of individuals across the world as the leading cause of irreversible blindness. The most common and only modifiable risk factor for developing glaucoma is elevated IOP, which is thought to be caused by impaired outflow of the aqueous humor. The reduction in outflow is thought to be due to dysfunction of the TM. ECM is an important component of the TM, surrounding and interacting with cells. SPARC, a protein that has been shown to modulate ECM in various tissues throughout the body, is strongly present in the TM, making it a point of interest in glaucoma research. Mice lacking SPARC have been shown to have a significantly lower IOP (approximately 15-20%). This suggests that a decreased amount of ECM in the TM leads to increased outflow and a lower IOP. SPARC has also been shown to be highly upregulated by TGFß2, an essential molecule that is elevated in the aqueous humor of glaucoma patients and causes ECM deposition within the TM in rodents, thereby leading to IOP elevation. Our first study explored the differences in outflow between WT and SPARC KO mice and whether outflow is linked with IOP. Our second study evaluated whether SPARC is an essential node in TGFß2-mediated ocular hypertension.

In the first study, fluorescent microbeads were used as a tracer to identify where outflow was occurring throughout the mouse eye; the presence of tracer in a specific region of the eye was interpreted as the presence of outflow in that region. A needle was placed into the frontal portion of the eye and the tracer was subsequently injected into the eye. After 45 minutes, the animal was sacrificed and the eye was removed. The eye tissue was then mounted out on a microscopic slide for further evaluation using confocal microscopy. The tissue was processed further for analysis with light and electron microscopy.

In the second study, adenovirus containing a gene insert that codes for TGFß2 or no gene insert (the control group) was injected into WT and mice lacking SPARC. IOPs were measured every other day for approximately 2 weeks. Some mice that were injected with the adenoviruses were then sacrificed, and the eye tissue was evaluated with immunofluorescence to determine the relative levels of protein concentration.

In eyes lacking SPARC, outflow was much more homogeneous than what was observed in WT eyes. Quantifying the area utilized for outflow, we determined that approximately 71% of the total area available for outflow was utilized by SPARC-null mice, while 55% of the total area available was used in wild-type mice. Outflow was much more continuous in the SPARC-null eye when examining the overall tracer pattern. Wild-type eyes displayed segmental flow, or flow that was punctuated in specific regions of the eye. When evaluating the association between outflow area and IOPs, a strong negative correlation was discovered ($R^2 = 0.72$). If a mouse's IOP was lower, its outflow area was greater. The electron microscopy data demonstrated that the less compact the TM tissue, the easier it was for the aqueous humor to exit the eye. Eyes lacking SPARC were also found to have smaller collagen fibrils, demonstrating that SPARC is important in ECM synthesis.

When TGFß2 was injected into WT eyes, IOP increased significantly for approximately two weeks. However, when TGFß2 was injected into SPARC-null eyes, IOP did not change significantly. Evaluation of injected tissue showed that 4 proteins were strongly elevated in WT eyes. However, only two of these were significantly elevated in injected SPARC-null eyes. Collagen IV and fibronectin were the two proteins that did not change, seeming to indicate that these two proteins are important in causing IOP elevation.

Our study demonstrates that SPARC plays an important role in modulating aqueous humor outflow, affecting the amount of TM utilized for outflow and IOP as well. Because of the role of SPARC in ECM modulation, this study implicates altered ECM morphology and compactness in the elevation of IOP. In addition, the discovery of various degrees of outflow throughout the mouse eye is a novel finding, underscoring its potential importance in mammalian evolution. The correlation data linking outflow area to IOP values is the first of its kind, indicating the strong relationship between the two. The second set of experiments demonstrated that SPARC is essential to TGFß2-mediated IOP elevation. Collagen IV and fibronectin appear to be essential to that process. Ultimately, this work highlights SPARC as an essential candidate for additional evaluation in glaucoma pathogenesis.

Acknowledgments

The author would like to thank his PI, Dr. Douglas J. Rhee, for his continuous support, guidance, and enthusiastic mentorship. The author would also like to thank Haiyan Gong for her valuable assistance with the microscopy portion of this work, as well as Mark Johnson, Jeffrey Ruberti, Allan Shepard, and Sandeep Menon for their advice regarding methodology. Finally, the author would like to thank the Harvard-MIT Health Sciences and Technology (HST) program at Harvard Medical School and the Howard Hughes Medical Institute (HHMI) Medical Research Fellows program for their financial support.

List of References

1. Rouland JF, Berdeaux G, Lafuma A. The economic burden of glaucoma and ocular hypertension: implications for patient management: a review. *Drugs Aging* 2005;22:315-321.
2. Klein BE, Klein R, Sponsel WE, et al. Prevalence of glaucoma. The Beaver Dam Eye Study. *Ophthalmology* 1992;99:1499-1504.
3. Leske MC, Connell AM, Schachat AP, Hyman L. The Barbados Eye Study. Prevalence of open angle glaucoma. *Arch Ophthalmol* 1994;112:821-829.
4. Nemesure B, Honkanen R, Hennis A, Wu SY, Leske MC. Incident open-angle glaucoma and intraocular pressure. *Ophthalmology* 2007;114:1810-1815.
5. Johnson M, Erickson K. Mechanisms and routes of aqueous humor drainage. In: Albert DM, Jakobiec FA (eds), *Principles and Practice of Ophthalmology.* Philadelphia: WB Saunders; 2000:2577-2595.
6. Grant WM. Experimental aqueous perfusion in enucleated human eyes. *Arch Ophthalmol* 1963;69:783-801.
7. Seiler T, Wollensak J. The resistance of the trabecular meshwork to aqueous humor outflow. *Graefes Arch Clin Exp Ophthalmol* 1985;223:88-91.
8. Bradley JM, Vranka J, Colvis CM, et al. Effect of matrix metalloproteinases activity on outflow in perfused human organ culture. *Invest Ophthalmol Vis Sci* 1998;39:2649-2658.
9. Bradley JM, Kelley MJ, Zhu X, Anderssohn AM, Alexander JP, Acott TS. Effects of mechanical stretching on trabecular matrix metalloproteinases. *Invest Ophthalmol Vis Sci* 2001;42:1505-1513.
10. Keller KE, Aga M, Bradley JM, Kelley MJ, Acott TS. Extracellular matrix turnover and outflow resistance. *Exp Eye Res* 2009;88:676-682.
11. Alvarado J, Murphy C, Juster R. Trabecular meshwork cellularity in primary open-angle glaucoma and nonglaucomatous normals. *Ophthalmology* 1984;91:564-579.
12. Keller KE, Acott TS. The Juxtacanalicular Region of Ocular Trabecular Meshwork: A Tissue with a Unique Extracellular Matrix and Specialized Function. *J Ocul Biol* 2013;1:3.
13. Johnson MC, Kamm RD. The role of Schlemm's canal in aqueous outflow from the human eye. *Invest Ophthalmol Vis Sci* 1983;24:320-325.
14. Rosenquist R, Epstein D, Melamed S, Johnson M, Grant WM. Outflow resistance of enucleated human eyes at two different perfusion pressures and different extents of trabeculotomy. *Curr Eye Res* 1989;8:1233-1240.
15. Minckler DS, Baerveldt G, Alfaro MR, Francis BA. Clinical results with the Trabectome for treatment of open-angle glaucoma. *Ophthalmology* 2005;112:962-967.
16. Maepea O, Bill A. Pressures in the juxtacanalicular tissue and Schlemm's canal in monkeys. *Exp Eye Res* 1992;54:879-883.
17. Maepea O, Bill A. The pressures in the episcleral veins, Schlemm's canal and the trabecular meshwork in monkeys: effects of changes in intraocular pressure. *Exp Eye Res* 1989;49:645-663.
18. Buller C, Johnson D. Segmental variability of the trabecular meshwork in normal and glaucomatous eyes. *Invest Ophthalmol Vis Sci* 1994;35:3841-3851.
19. Gong H, Ruberti J, Overby D, Johnson M, Freddo TF. A new view of the human trabecular meshwork using quick-freeze, deep-etch electron microscopy. *Exp Eye Res* 2002;75:347-358.
20. Alvarado JA, Yun AJ, Murphy CG. Juxtacanalicular tissue in primary open angle glaucoma and in nonglaucomatous normals. *Arch Ophthalmol* 1986;104:1517-1528.

21. Lutjen-Drecoll E, Shimizu T, Rohrbach M, Rohen JW. Quantitative analysis of 'plaque material' in the inner- and outer wall of Schlemm's canal in normal- and glaucomatous eyes. *Exp Eye Res* 1986;42:443-455.
22. Gottanka J, Johnson DH, Martus P, Lutjen-Drecoll E. Severity of optic nerve damage in eyes with POAG is correlated with changes in the trabecular meshwork. *J Glaucoma* 1997;6:123-132.
23. Overby DR, Stamer WD, Johnson M. The changing paradigm of outflow resistance generation: towards synergistic models of the JCT and inner wall endothelium. *Exp Eye Res* 2009;88:656-670.
24. Lu Z, Overby DR, Scott PA, Freddo TF, Gong H. The mechanism of increasing outflow facility by rho-kinase inhibition with Y-27632 in bovine eyes. *Exp Eye Res* 2008;86:271-281.
25. Johnstone MA, Grant WG. Pressure-dependent changes in structures of the aqueous outflow system of human and monkey eyes. *Am J Ophthalmol* 1973;75:365-383.
26. Hann CR, Bahler CK, Johnson DH. Cationic ferritin and segmental flow through the trabecular meshwork. *Invest Ophthalmol Vis Sci* 2005;46:1-7.
27. Francis BA, Winarko J. Ab interno Schlemm's canal surgery: trabectome and i-stent. *Dev Ophthalmol* 2012;50:125-136.
28. Zhang Y, Toris CB, Liu Y, Ye W, Gong H. Morphological and hydrodynamic correlates in monkey eyes with laser induced glaucoma. *Exp Eye Res* 2009;89:748-756.
29. Lindsey JD, Weinreb RN. Identification of the mouse uveoscleral outflow pathway using fluorescent dextran. *Invest Ophthalmol Vis Sci* 2002;43:2201-2205.
30. Lindsey JD, Hofer A, Wright KN, Weinreb RN. Partitioning of the aqueous outflow in rat eyes. *Invest Ophthalmol Vis Sci* 2009;50:5754-5758.
31. Bernd AS, Aihara M, Lindsey JD, Weinreb RN. Influence of molecular weight on intracameral dextran movement to the posterior segment of the mouse eye. *Invest Ophthalmol Vis Sci* 2004;45:480-484.
32. Crowston JG, Aihara M, Lindsey JD, Weinreb RN. Effect of latanoprost on outflow facility in the mouse. *Invest Ophthalmol Vis Sci* 2004;45:2240-2245.
33. Camelo S, Shanley AC, Voon AS, McMenamin PG. An intravital and confocal microscopic study of the distribution of intracameral antigen in the aqueous outflow pathways and limbus of the rat eye. *Exp Eye Res* 2004;79:455-464.
34. Clark AF, Wilson K, McCartney MD, Miggans ST, Kunkle M, Howe W. Glucocorticoid-induced formation of cross-linked actin networks in cultured human trabecular meshwork cells. *Invest Ophthalmol Vis Sci* 1994;35:281-294.
35. Filla MS, Woods A, Kaufman PL, Peters DM. Beta1 and beta3 integrins cooperate to induce syndecan-4-containing cross-linked actin networks in human trabecular meshwork cells. *Invest Ophthalmol Vis Sci* 2006;47:1956-1967.
36. O'Reilly S, Pollock N, Currie L, Paraoan L, Clark AF, Grierson I. Inducers of cross-linked actin networks in trabecular meshwork cells. *Invest Ophthalmol Vis Sci* 2011;52:7316-7324.
37. Liang LL, Epstein DL, de Kater AW, Shahsafaei A, Erickson-Lamy KA. Ethacrynic acid increases facility of outflow in the human eye in vitro. *Arch Ophthalmol* 1992;110:106-109.
38. Epstein DL, Roberts BC, Skinner LL. Nonsulfhydryl-reactive phenoxyacetic acids increase aqueous humor outflow facility. *Invest Ophthalmol Vis Sci* 1997;38:1526-1534.
39. Peterson JA, Tian B, Bershadsky AD, et al. Latrunculin-A increases outflow facility in the monkey. *Invest Ophthalmol Vis Sci* 1999;40:931-941.

40. Okka M, Tian B, Kaufman PL. Effect of low-dose latrunculin B on anterior segment physiologic features in the monkey eye. *Arch Ophthalmol* 2004;122:1482-1488.
41. Honjo M, Inatani M, Kido N, et al. Effects of protein kinase inhibitor, HA1077, on intraocular pressure and outflow facility in rabbit eyes. *Arch Ophthalmol* 2001;119:1171-1178.
42. Tanihara H, Inoue T, Yamamoto T, Kuwayama Y, Abe H, Araie M. Phase 1 Clinical Trials of a Selective Rho Kinase Inhibitor, K-115. *JAMA Ophthalmol* 2013;1-8.
43. Pichler RH, Hugo C, Shankland SJ, et al. SPARC is expressed in renal interstitial fibrosis and in renal vascular injury. *Kidney Int* 1996;50:1978-1989.
44. Nakken KE, Nygard S, Haaland T, et al. Multiple inflammatory-, tissue remodelling- and fibrosis genes are differentially transcribed in the livers of Abcb4 (-/ -) mice harbouring chronic cholangitis. *Scand J Gastroenterol* 2007;42:1245-1255.
45. Barker TH, Baneyx G, Cardo-Vila M, et al. SPARC regulates extracellular matrix organization through its modulation of integrin-linked kinase activity. *J Biol Chem* 2005;280:36483-36493.
46. Zhou X, Tan FK, Guo X, Arnett FC. Attenuation of collagen production with small interfering RNA of SPARC in cultured fibroblasts from the skin of patients with scleroderma. *Arthritis Rheum* 2006;54:2626-2631.
47. Bradshaw AD, Puolakkainen P, Dasgupta J, Davidson JM, Wight TN, Helene Sage E. SPARC-null mice display abnormalities in the dermis characterized by decreased collagen fibril diameter and reduced tensile strength. *J Invest Dermatol* 2003;120:949-955.
48. Bradshaw AD, Reed MJ, Sage EH. SPARC-null mice exhibit accelerated cutaneous wound closure. *J Histochem Cytochem* 2002;50:1-10.
49. Puolakkainen P, Bradshaw AD, Kyriakides TR, et al. Compromised production of extracellular matrix in mice lacking secreted protein, acidic and rich in cysteine (SPARC) leads to a reduced foreign body reaction to implanted biomaterials. *Am J Pathol* 2003;162:627-635.
50. Delany AM, Amling M, Priemel M, Howe C, Baron R, Canalis E. Osteopenia and decreased bone formation in osteonectin-deficient mice. *J Clin Invest* 2000;105:1325.
51. Tomarev SI, Wistow G, Raymond V, Dubois S, Malyukova I. Gene expression profile of the human trabecular meshwork: NEIBank sequence tag analysis. *Invest Ophthalmol Vis Sci* 2003;44:2588-2596.
52. Vittal V, Rose A, Gregory KE, Kelley MJ, Acott TS. Changes in gene expression by trabecular meshwork cells in response to mechanical stretching. *Invest Ophthalmol Vis Sci* 2005;46:2857-2868.
53. Yan Q, Clark JI, Sage EH. Expression and characterization of SPARC in human lens and in the aqueous and vitreous humors. *Exp Eye Res* 2000;71:81-90.
54. Berryhill BL, Kane B, Stramer BM, Fini ME, Hassell JR. Increased SPARC accumulation during corneal repair. *Exp Eye Res* 2003;77:85-92.
55. Kantorow M, Huang Q, Yang XJ, et al. Increased expression of osteonectin/SPARC mRNA and protein in age-related human cataracts and spatial expression in the normal human lens. *Mol Vis* 2000;6:24-29.
56. Rhee DJ, Haddadin RI, Kang MH, Oh DJ. Matricellular proteins in the trabecular meshwork. *Exp Eye Res* 2009;88:694-703.
57. Rhee DJ, Fariss RN, Brekken R, Sage EH, Russell P. The matricellular protein SPARC is expressed in human trabecular meshwork. *Exp Eye Res* 2003;77:601-607.
58. Haddadin RI, Oh DJ, Kang MH, et al. SPARC-null mice exhibit lower intraocular pressures. *Invest Ophthalmol Vis Sci* 2009;50:3771-3777.

59. Oh DJ, Kang MH, Ooi YH, Choi KR, Sage EH, Rhee DJ. Overexpression of SPARC in human trabecular meshwork increases intraocular pressure and alters extracellular matrix. *Invest Ophthalmol Vis Sci* 2013;54:3309-3319.
60. Bataller R, Brenner DA. Liver fibrosis. *J Clin Invest* 2005;115:209-218.
61. Liu Y. Renal fibrosis: new insights into the pathogenesis and therapeutics. *Kidney Int* 2006;69:213-217.
62. Bollinger KE, Crabb JS, Yuan X, Putliwala T, Clark AF, Crabb JW. Quantitative proteomics: TGFbeta(2) signaling in trabecular meshwork cells. *Invest Ophthalmol Vis Sci* 2011;52:8287-8294.
63. Gottanka J, Chan D, Eichhorn M, Lutjen-Drecoll E, Ethier CR. Effects of TGF-beta2 in perfused human eyes. *Invest Ophthalmol Vis Sci* 2004;45:153-158.
64. Shepard AR, Millar JC, Pang IH, Jacobson N, Wang WH, Clark AF. Adenoviral gene transfer of active human transforming growth factor-{beta}2 elevates intraocular pressure and reduces outflow facility in rodent eyes. *Invest Ophthalmol Vis Sci* 2010;51:2067-2076.
65. Fuchshofer R, Tamm ER. The role of TGF-beta in the pathogenesis of primary open-angle glaucoma. *Cell Tissue Res* 2012;347:279-290.
66. Inatani M, Tanihara H, Katsuta H, Honjo M, Kido N, Honda Y. Transforming growth factor-beta 2 levels in aqueous humor of glaucomatous eyes. *Graefes Arch Clin Exp Ophthalmol* 2001;239:109-113.
67. Ochiai Y, Ochiai H. Higher concentration of transforming growth factor-beta in aqueous humor of glaucomatous eyes and diabetic eyes. *Jpn J Ophthalmol* 2002;46:249-253.
68. Picht G, Welge-Luessen U, Grehn F, Lutjen-Drecoll E. Transforming growth factor beta 2 levels in the aqueous humor in different types of glaucoma and the relation to filtering bleb development. *Graefes Arch Clin Exp Ophthalmol* 2001;239:199-207.
69. Tripathi RC, Li J, Chan WF, Tripathi BJ. Aqueous humor in glaucomatous eyes contains an increased level of TGF-beta 2. *Exp Eye Res* 1994;59:723-727.
70. Tovar-Vidales T, Clark AF, Wordinger RJ. Transforming growth factor-beta2 utilizes the canonical Smad-signaling pathway to regulate tissue transglutaminase expression in human trabecular meshwork cells. *Exp Eye Res* 2011;93:442-451.
71. Fleenor DL, Shepard AR, Hellberg PE, Jacobson N, Pang IH, Clark AF. TGFbeta2-induced changes in human trabecular meshwork: implications for intraocular pressure. *Invest Ophthalmol Vis Sci* 2006;47:226-234.
72. Fuchshofer R, Yu AH, Welge-Lussen U, Tamm ER. Bone morphogenetic protein-7 is an antagonist of transforming growth factor-beta2 in human trabecular meshwork cells. *Invest Ophthalmol Vis Sci* 2007;48:715-726.
73. Li J, Tripathi BJ, Tripathi RC. Modulation of pre-mRNA splicing and protein production of fibronectin by TGF-beta2 in porcine trabecular cells. *Invest Ophthalmol Vis Sci* 2000;41:3437-3443.
74. Zhao X, Ramsey KE, Stephan DA, Russell P. Gene and protein expression changes in human trabecular meshwork cells treated with transforming growth factor-beta. *Invest Ophthalmol Vis Sci* 2004;45:4023-4034.
75. Zhao X, Russell P. Versican splice variants in human trabecular meshwork and ciliary muscle. *Mol Vis* 2005;11:603-608.
76. Wordinger RJ, Fleenor DL, Hellberg PE, et al. Effects of TGF-beta2, BMP-4, and gremlin in the trabecular meshwork: implications for glaucoma. *Invest Ophthalmol Vis Sci* 2007;48:1191-1200.

77. Kang MH, Oh DJ, Rhee DJ. Regulation of SPARC by Transforming Growth Factor β-2 in Human Trabecular Meshwork. *Invest Ophthalmol Vis Sci* 2013;54:2523-2532.
78. Yu AL, Birke K, Moriniere J, Welge-Lussen U. TGF-{beta}2 induces senescence-associated changes in human trabecular meshwork cells. *Invest Ophthalmol Vis Sci* 2010;51:5718-5723.
79. Richter M, Krauss AH, Woodward DF, Lutjen-Drecoll E. Morphological changes in the anterior eye segment after long-term treatment with different receptor selective prostaglandin agonists and a prostamide. *Invest Ophthalmol Vis Sci* 2003;44:4419-4426.
80. Weinreb RN, Kashiwagi K, Kashiwagi F, Tsukahara S, Lindsey JD. Prostaglandins increase matrix metalloproteinase release from human ciliary smooth muscle cells. *Invest Ophthalmol Vis Sci* 1997;38:2772-2780.
81. Rohen JW, Lutjen-Drecoll E, Flugel C, Meyer M, Grierson I. Ultrastructure of the trabecular meshwork in untreated cases of primary open-angle glaucoma (POAG). *Exp Eye Res* 1993;56:683-692.
82. Aihara M, Lindsey JD, Weinreb RN. Ocular hypertension in mice with a targeted type I collagen mutation. *Invest Ophthalmol Vis Sci* 2003;44:1581-1585.
83. Burgess A, Vigneron S, Brioudes E, Labbe JC, Lorca T, Castro A. Loss of human Greatwall results in G2 arrest and multiple mitotic defects due to deregulation of the cyclin B-Cdc2/PP2A balance. *Proc Natl Acad Sci U S A* 2010;107:12564-12569.
84. Potapova TA, Sivakumar S, Flynn JN, Li R, Gorbsky GJ. Mitotic progression becomes irreversible in prometaphase and collapses when Wee1 and Cdc25 are inhibited. *Mol Biol Cell* 2011;22:1191-1206.
85. Aihara M, Lindsey JD, Weinreb RN. Reduction of intraocular pressure in mouse eyes treated with latanoprost. *Invest Ophthalmol Vis Sci* 2002;43:146-150.
86. Savinova OV, Sugiyama F, Martin JE, et al. Intraocular pressure in genetically distinct mice: an update and strain survey. *BMC Genet* 2001;2:12.
87. Lohr C, Kunding AH, Bhatia VK, Stamou D. Constructing size distributions of liposomes from single-object fluorescence measurements. *Methods Enzymol* 2009;465:143-160.
88. Downey MJ, Jeziorska DM, Ott S, et al. Extracting fluorescent reporter time courses of cell lineages from high-throughput microscopy at low temporal resolution. *PLoS One* 2011;6:e27886.
89. Hernandez-Garcia CM, Chiera JM, Finer JJ. Robotics and dynamic image analysis for studies of gene expression in plant tissues. *J Vis Exp* 2010.
90. Haddadin RI, Oh DJ, Kang MH, et al. Thrombospondin-1 (TSP1)-null and TSP2-null mice exhibit lower intraocular pressures. *Invest Ophthalmol Vis Sci* 2012;53:6708-6717.
91. Bornstein P, Kyriakides TR, Yang Z, Armstrong LC, Birk DE. Thrombospondin 2 modulates collagen fibrillogenesis and angiogenesis. *J Investig Dermatol Symp Proc* 2000;5:61-66.
92. Kadler KE, Hill A, Canty-Laird EG. Collagen fibrillogenesis: fibronectin, integrins, and minor collagens as organizers and nucleators. *Curr Opin Cell Biol* 2008;20:495-501.
93. Kalamajski S, Oldberg A. The role of small leucine-rich proteoglycans in collagen fibrillogenesis. *Matrix Biol* 2010;29:248-253.
94. Fuchshofer R, Tamm ER. Modulation of extracellular matrix turnover in the trabecular meshwork. *Exp Eye Res* 2009;88:683-688.
95. Aihara M, Lindsey JD, Weinreb RN. Aqueous humor dynamics in mice. *Invest Ophthalmol Vis Sci* 2003;44:5168-5173.

96. Millar JC, Clark AF, Pang IH. Assessment of aqueous humor dynamics in the mouse by a novel method of constant-flow infusion. *Invest Ophthalmol Vis Sci* 2011;52:685-694.
97. Pease ME, Cone FE, Gelman S, Son JL, Quigley HA. Calibration of the TonoLab tonometer in mice with spontaneous or experimental glaucoma. *Invest Ophthalmol Vis Sci* 2011;52:858-864.
98. Hiscott P, Schlotzer-Schrehardt U, Naumann GO. Unexpected expression of thrombospondin 1 by corneal and iris fibroblasts in the pseudoexfoliation syndrome. *Hum Pathol* 1996;27:1255-1258.
99. Wordinger RJ, Clark AF, Agarwal R, et al. Cultured human trabecular meshwork cells express functional growth factor receptors. *Invest Ophthalmol Vis Sci* 1998;39:1575-1589.
100. Cao Y, Wei H, Da B, Huang Y. Effect of transforming growth factor-beta 2 on phagocytosis in cultured bovine trabecular meshwork cells. *J Tongji Med Univ* 2001;21:318-320.
101. Junglas B, Yu AH, Welge-Lussen U, Tamm ER, Fuchshofer R. Connective tissue growth factor induces extracellular matrix deposition in human trabecular meshwork cells. *Exp Eye Res* 2009;88:1065-1075.
102. Dan J, Belyea D, Gertner G, Leshem I, Lusky M, Miskin R. Plasminogen activator inhibitor-1 in the aqueous humor of patients with and without glaucoma. *Arch Ophthalmol* 2005;123:220-224.
103. Fuchshofer R, Welge-Lussen U, Lutjen-Drecoll E. The effect of TGF-beta2 on human trabecular meshwork extracellular proteolytic system. *Exp Eye Res* 2003;77:757-765.
104. Barker TH, Framson P, Puolakkainen PA, Reed M, Funk SE, Sage EH. Matricellular homologs in the foreign body response: hevin suppresses inflammation, but hevin and SPARC together diminish angiogenesis. *Am J Pathol* 2005;166:923-933.
105. Martinek N, Shahab J, Saathoff M, Ringuette M. Haemocyte-derived SPARC is required for collagen-IV-dependent stability of basal laminae in Drosophila embryos. *J Cell Sci* 2008;121:1671-1680.
106. Maurer P, Gohring W, Sasaki T, Mann K, Timpl R, Nischt R. Recombinant and tissue-derived mouse BM-40 bind to several collagen types and have increased affinities after proteolytic activation. *Cell Mol Life Sci* 1997;53:478-484.
107. Jia L, Cepurna WO, Johnson EC, Morrison JC. Effect of general anesthetics on IOP in rats with experimental aqueous outflow obstruction. *Invest Ophthalmol Vis Sci* 2000;41:3415-3419.
108. Jones L, Sung V, Lascaratos G, Nagi H, Holder R. Intraocular pressures after ketamine and sevoflurane in children with glaucoma undergoing examination under anaesthesia. *Br J Ophthalmol* 2010;94:33-35.
109. Blumberg D, Congdon N, Jampel H, et al. The effects of sevoflurane and ketamine on intraocular pressure in children during examination under anesthesia. *Am J Ophthalmol* 2007;143:494-499.
110. Swaminathan SS, Oh DJ, Kang MH, et al. Secreted Protein, Acidic and Rich in Cysteine (SPARC)-Null Mice Exhibit More Uniform Outflow. *Invest Ophthalmol Vis Sci* 2013;54:2035-2047.
111. Hijazi Y, Boulieu R. Contribution of CYP3A4, CYP2B6, and CYP2C9 isoforms to N-demethylation of ketamine in human liver microsomes. *Drug Metab Dispos* 2002;30:853-858.
112. Kokki H. Nonsteroidal anti-inflammatory drugs for postoperative pain: a focus on children. *Paediatr Drugs* 2003;5:103-123.
113. Perisho JA, Buechel DR, Miller RD. The effect of diazepam (Valium) on minimum alveolar anaesthetic requirement (MAC) in man. *Can Anaesth Soc J* 1971;18:536-540.

114. Wang JC, Lai S, Guo X, et al. Attenuation of fibrosis in vitro and in vivo with SPARC siRNA. *Arthritis Res Ther* 2010;12:R60.
115. Sangaletti S, Tripodo C, Cappetti B, et al. SPARC oppositely regulates inflammation and fibrosis in bleomycin-induced lung damage. *Am J Pathol* 2011;179:3000-3010.
116. Gaudana R, Ananthula HK, Parenky A, Mitra AK. Ocular drug delivery. *Aaps J* 2010;12:348-360.
117. Whitlock NA, McKnight B, Corcoran KN, Rodriguez LA, Rice DS. Increased intraocular pressure in mice treated with dexamethasone. *Invest Ophthalmol Vis Sci* 2010;51:6496-6503.
118. Kumar S, Shah S, Deutsch ER, Tang HM, Danias J. Triamcinolone acetonide decreases outflow facility in C57BL/6 mouse eyes. *Invest Ophthalmol Vis Sci* 2013;54:1280-1287.
119. Borras T, Tamm ER, Zigler JS, Jr. Ocular adenovirus gene transfer varies in efficiency and inflammatory response. *Invest Ophthalmol Vis Sci* 1996;37:1282-1293.
120. Tursz T, Cesne AL, Baldeyrou P, et al. Phase I study of a recombinant adenovirus-mediated gene transfer in lung cancer patients. *J Natl Cancer Inst* 1996;88:1857-1863.
121. Budenz DL, Bennett J, Alonso L, Maguire A. In vivo gene transfer into murine corneal endothelial and trabecular meshwork cells. *Invest Ophthalmol Vis Sci* 1995;36:2211-2215.
122. Bennett J, Maguire AM. Gene therapy for ocular disease. *Mol Ther* 2000;1:501-505.
123. Yan H, Cui J, Wang Y, Yu Y. Comparison of the effects between intravitreal and periocular injections of adenoviral vectored pigment epithelium-derived factor on suppressing choroidal neovascularization in rats. *Ophthalmic Res* 2013;49:81-89.
124. McDowell CM, Luan T, Zhang Z, et al. Mutant human myocilin induces strain specific differences in ocular hypertension and optic nerve damage in mice. *Exp Eye Res* 2012;100:65-72.
125. Mao W, Millar JC, Wang WH, et al. Existence of the canonical Wnt signaling pathway in the human trabecular meshwork. *Invest Ophthalmol Vis Sci* 2012;53:7043-7051.

Figures and Tables

Note: Figures 3-11 are reproduced from a previous publication[110]. The Association for Research in Vision and Ophthalmology, the copyright holder, has granted permission for their reproduction.

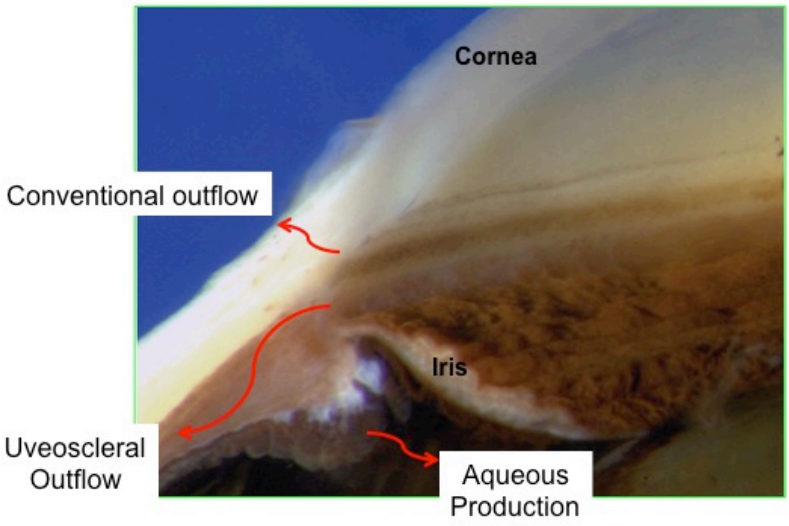

Figure 1. Diagram displaying the iridocorneal angle formed between the iris and cornea. Aqueous humor is produced by the ciliary body, after which the aqueous enters the anterior chamber and exits either via the conventional or uveoscleral outflow pathways (Image courtesy of DJ Rhee.)

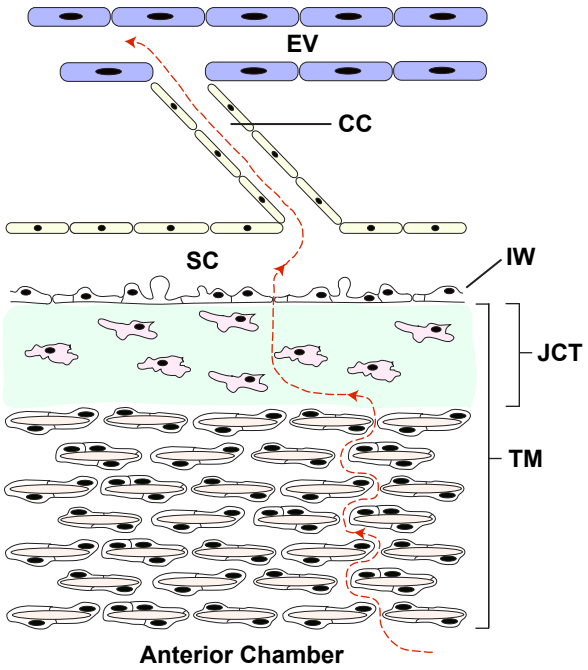

Figure 2. Schematic of the conventional outflow pathway. Arrows indicate the direction of aqueous flow. The fluid moves from the anterior chamber into the trabecular meshwork (TM), through the cells and extracellular matrix (green) of the juxtacanalicular tissue (JCT), into Schlemm's canal (SC) via the inner wall (IW), into collector channels, and ultimately into episcleral veins. The aqueous humor then joins the general venous circulation.

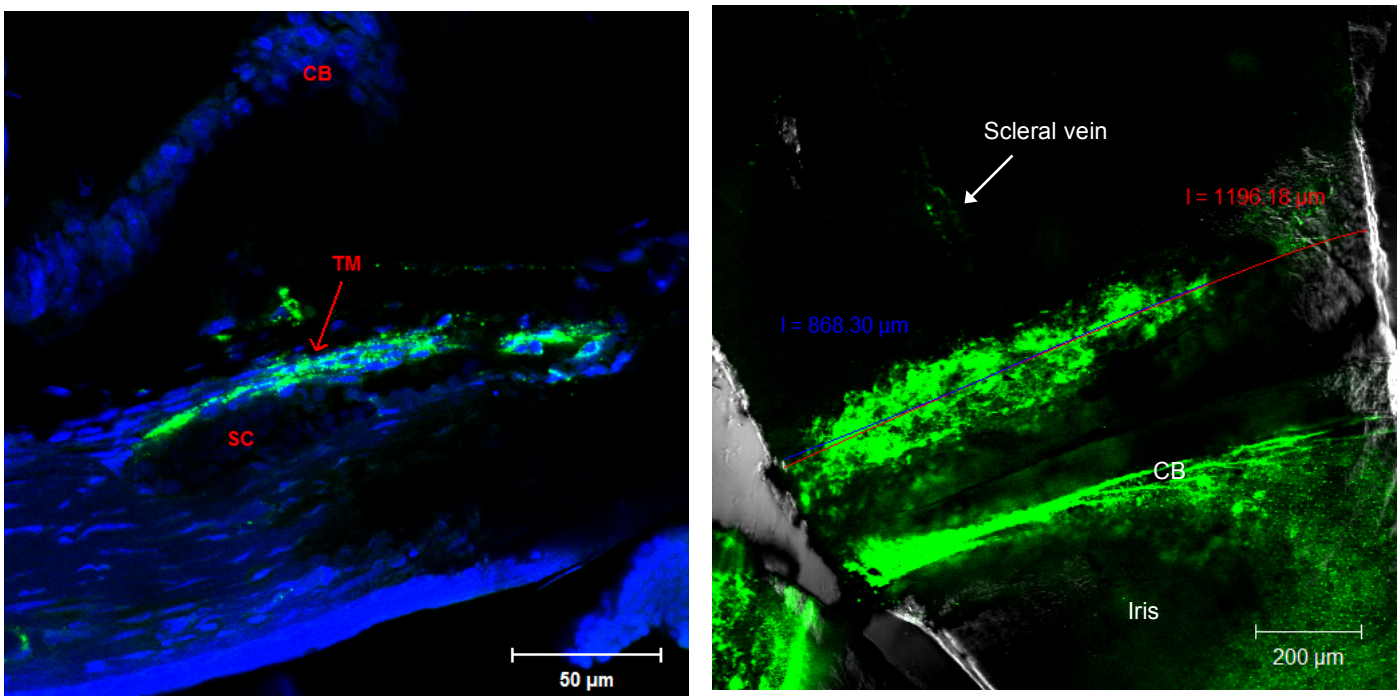

(A) (B)

Figure 3. Sample WT image of: (A) confocal microscopy with a radial section. Schlemm's canal (SC), trabecular meshwork (TM), and ciliary body (CB) are labeled. Cells have been stained with the blue TO-PRO-3 dye, while the fluorescent microspheres are green. (B) FL (blue) and TL (red) measurements from the en face image. In terms of orientation, the tissue in (A) is being viewed on the orthogonal in (B). PEFL for this specific tissue section can be calculated from FL and TL (here, PEFL = 868.30/1196.18 * 100% = 72.59%.) The fluorescence seen in the iris and ciliary body (CB) is due to auto-fluorescence. Tracer can also be seen in the scleral vein, indicating that the microbeads traverse the normal outflow pattern.

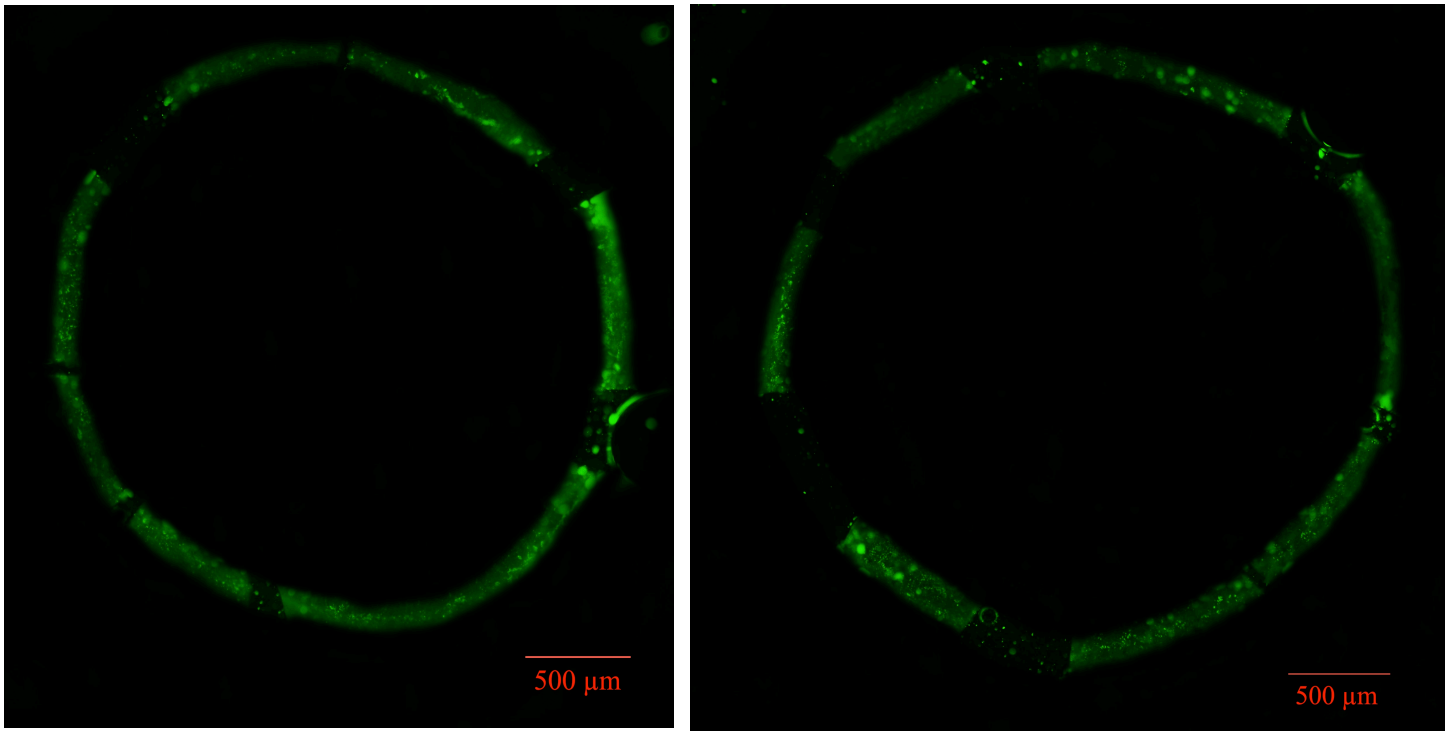

(A) (B)

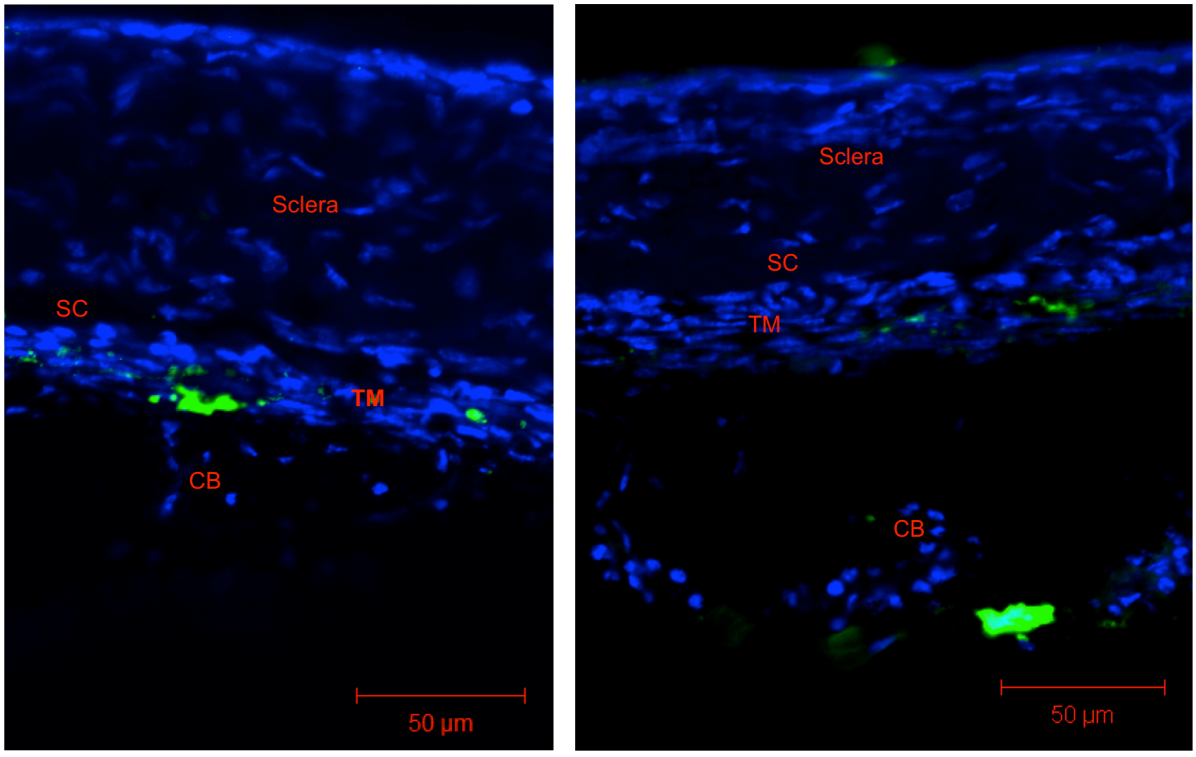

(C) (D)

Figure 4. Representative en face images of (A) WT and (B) KO eyes bathed in the microbead solution. Due to the significant amount of background from tracer binding the cornea and sclera, the central and peripheral portions of the images were removed. (C, D) Frontal confocal sections of WT and KO tissue, respectively, with sclera, trabecular meshwork (TM), Schlemm's canal (SC), and ciliary body (CB) labeled. Tracer accumulates mostly among the superficial–intermediate portions of the TM, rarely approaching SC.

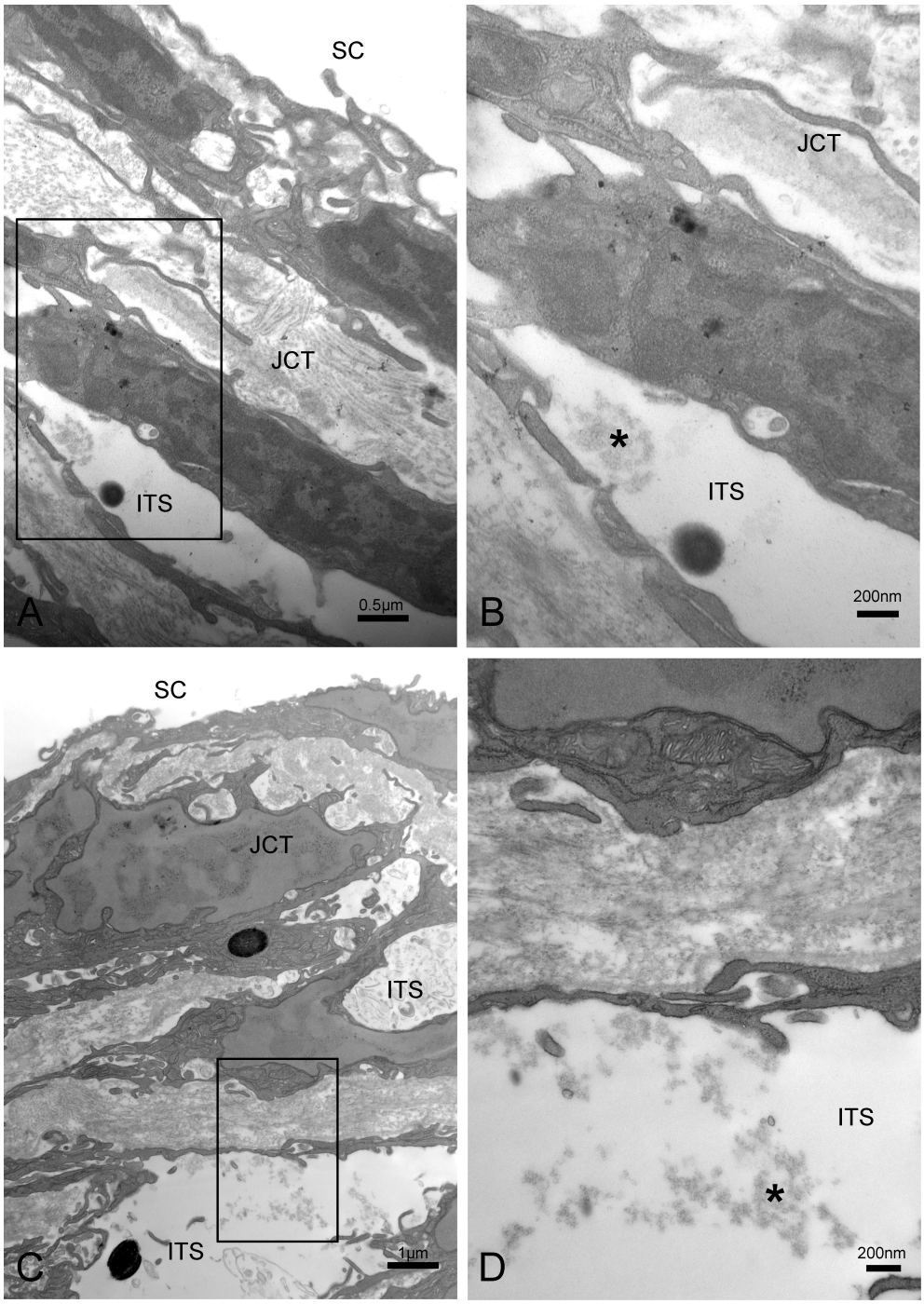

Figure 5. (A, B) Electron microscopy of WT tissue TM with Schlemm's canal (SC), juxtacanalicular connective tissue (JCT), and intertrabecular space (ITS) labeled. The black box region in (A) is magnified in (B). Microbeads (*) were found in the open spaces within the ITS. (C, D) Electron microscopy of KO tissue TM with SC, JCT, and ITS labeled. The black box region in (C) is magnified in (D). Microbeads (*) were again found in open spaces between trabecular beams.

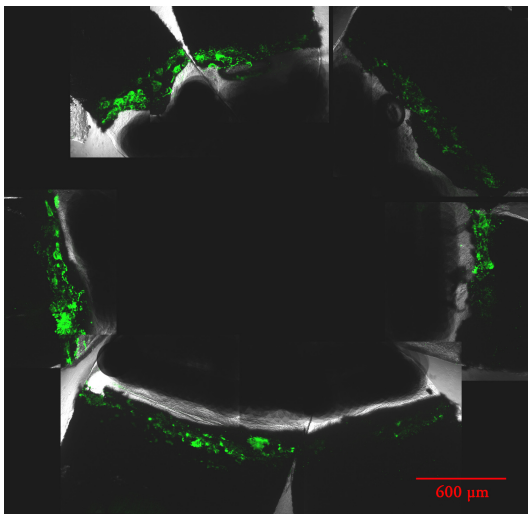
600 µm

(A)

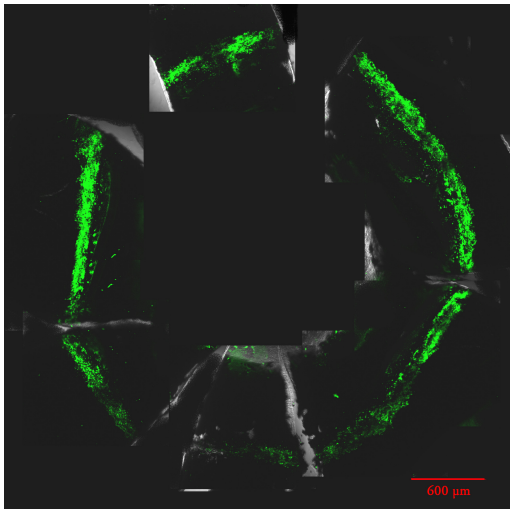
600 µm

(B)

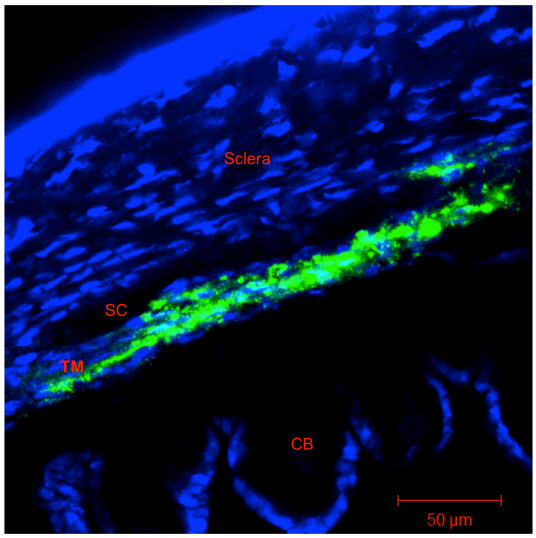
Sclera
SC
TM
CB
50 µm

(C)

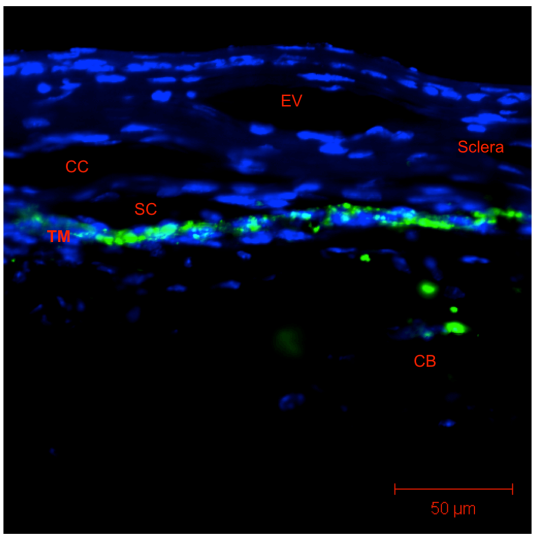
EV
Sclera
CC
SC
TM
CB
50 µm

(D)

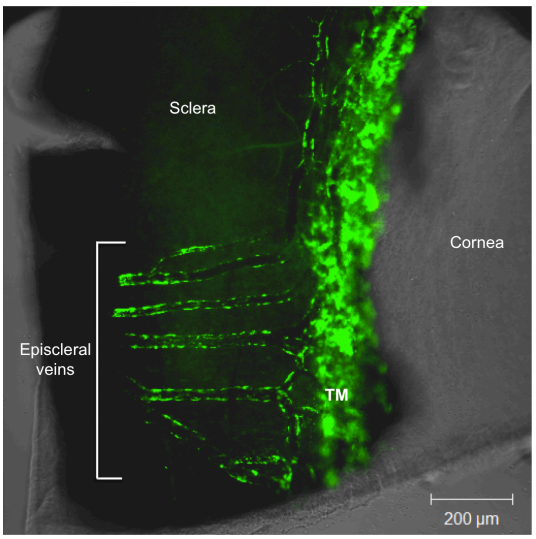
Sclera
Cornea
Episcleral veins
TM
200 µm

(E)

Figure 6. (A, B) Representative pair of matched WT and KO eyes. Confocal microscopy was completed en face through the corneal side. Tracer bead distribution in the TM of WT eyes was heterogeneous. A more homogeneous fluorescence pattern was observed in SPARC KO eyes, reflecting more uniform outflow. Gray portions of these images are from the projection of the brightfield lamp on the tissue and medium. Central portions of these images were removed due to iris autofluorescence. (C, D) Representative confocal microscopy of frontal sections of WT and KO high-tracer sections, respectively. Sclera, trabecular meshwork (TM), Schlemm's canal (SC), ciliary body (CB), collector channel (CC), and episcleral vein (EV) are labeled. Tracer is strongly present throughout the TM. Tracer can also be noted within SC. (E) En face image of a high-tracer section demonstrating microbeads within the TM and along the walls of episcleral veins.

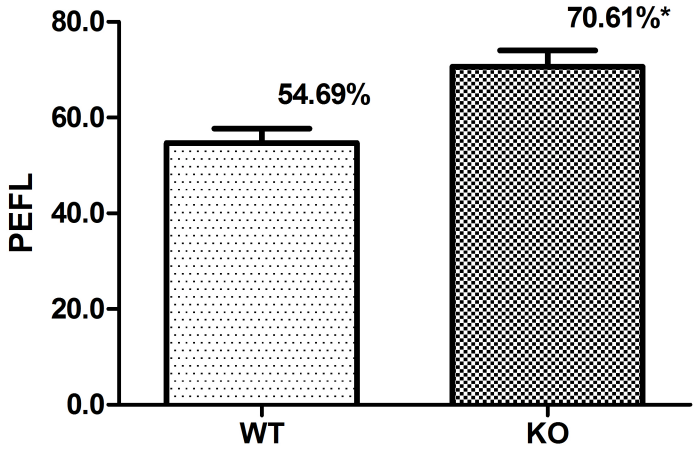

Figure 7. Percentage effective filtration length (PEFL) values in WT and KO eyes with SEM error bars. KO PEFL was significantly higher (*) than WT PEFL (N=11 pairs, $p<0.005$).

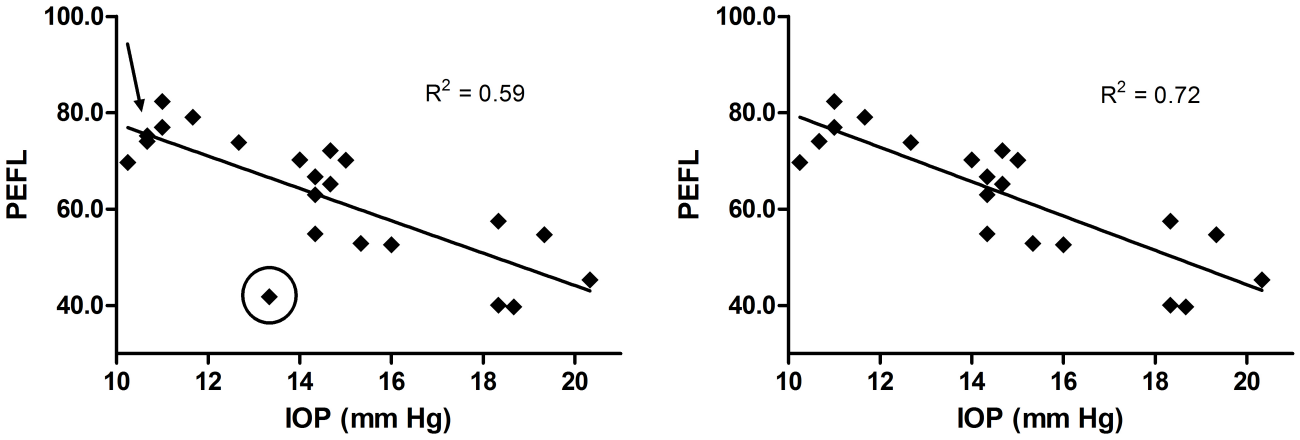

Figure 8. (A) IOP-PEFL correlation (N=20, $p<0.0001$). The outlier (circle) and its matched point (arrow) are identified. (B) IOP-PEFL correlation with these points removed. R^2 increases significantly.

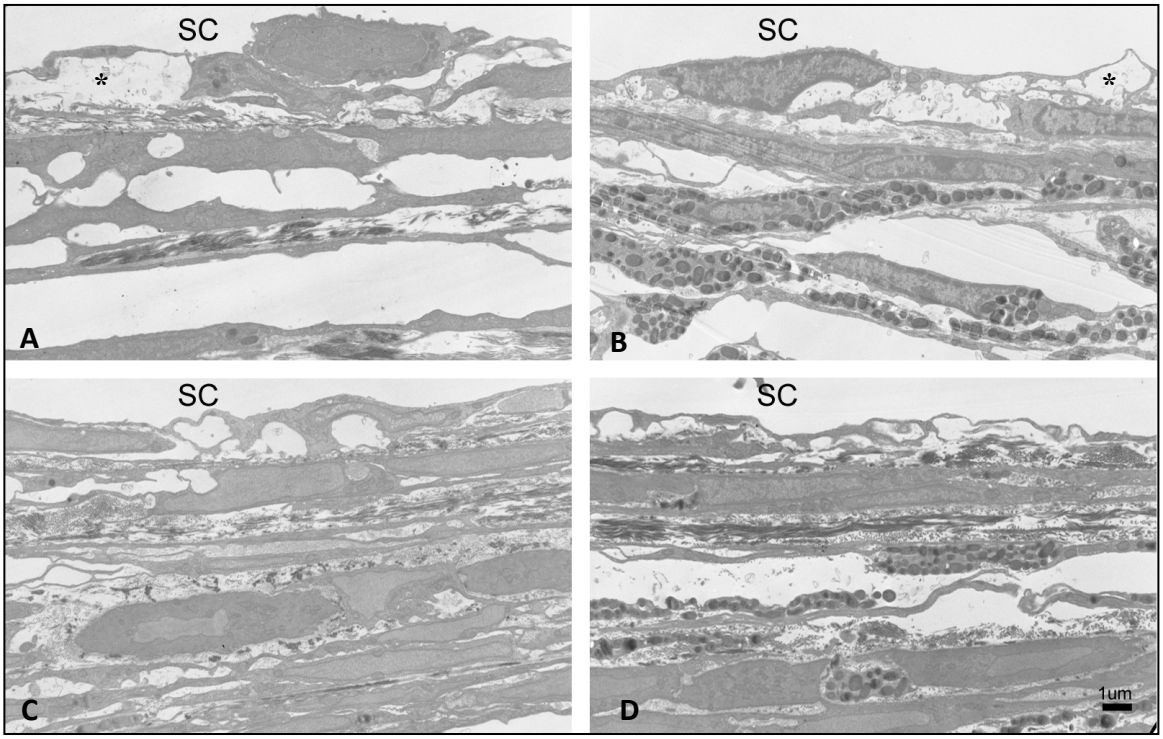

Figure 9. Representative EM images of the four conditions with Schlemm's canal (SC) labeled. (A) TM of a WT high-tracer region. Giant vacuole (*) labeled. (B) TM of a KO high-tracer region. Again, a vacuole can be seen. (C) TM of a WT low-tracer region, which appears quite compact. (D) TM of a KO low-tracer region, which is compact once again.

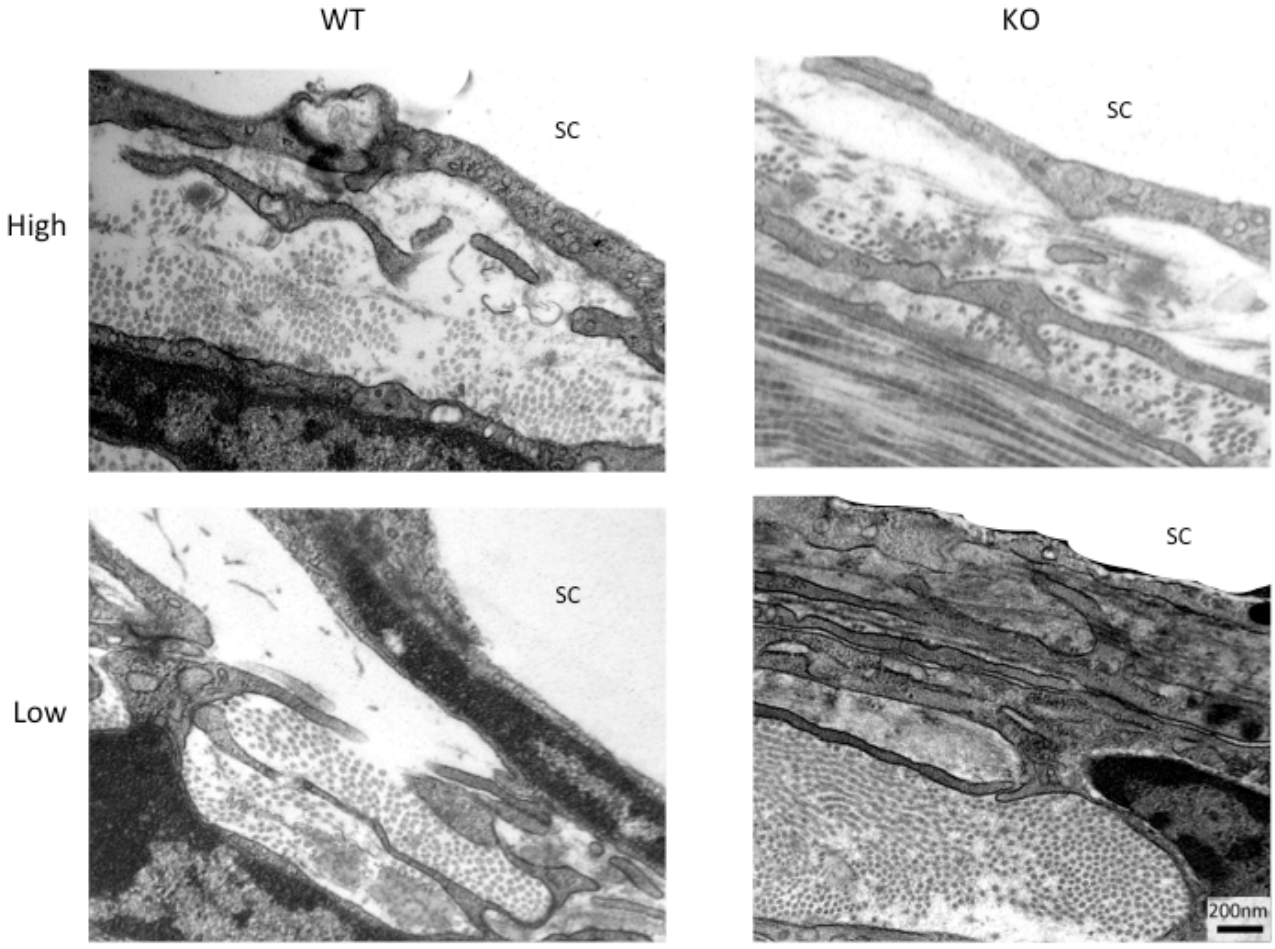

(A)

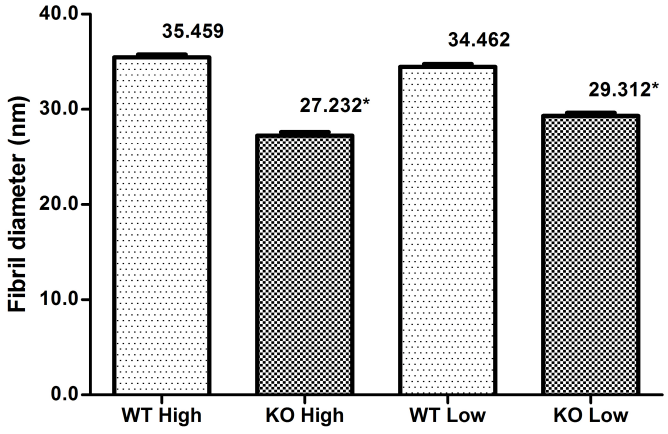

(B)

Figure 10. (A) Representative EM images of collagen fibrils in WT & KO high and low-tracer regions. Cross-sections of the fibrils within the JCT can be observed. Schlemm's Canal (SC) is labeled. (B) Comparison of average fibril diameter values between high & low-tracer regions of WT & KO tissue with SEM error bars. A total of 300 fibrils per eye derived from 5 different sections of JCT were assessed. Both KO high and low-tracer values were significantly decreased compared to those of WT (N=3; $p<0.0005$).

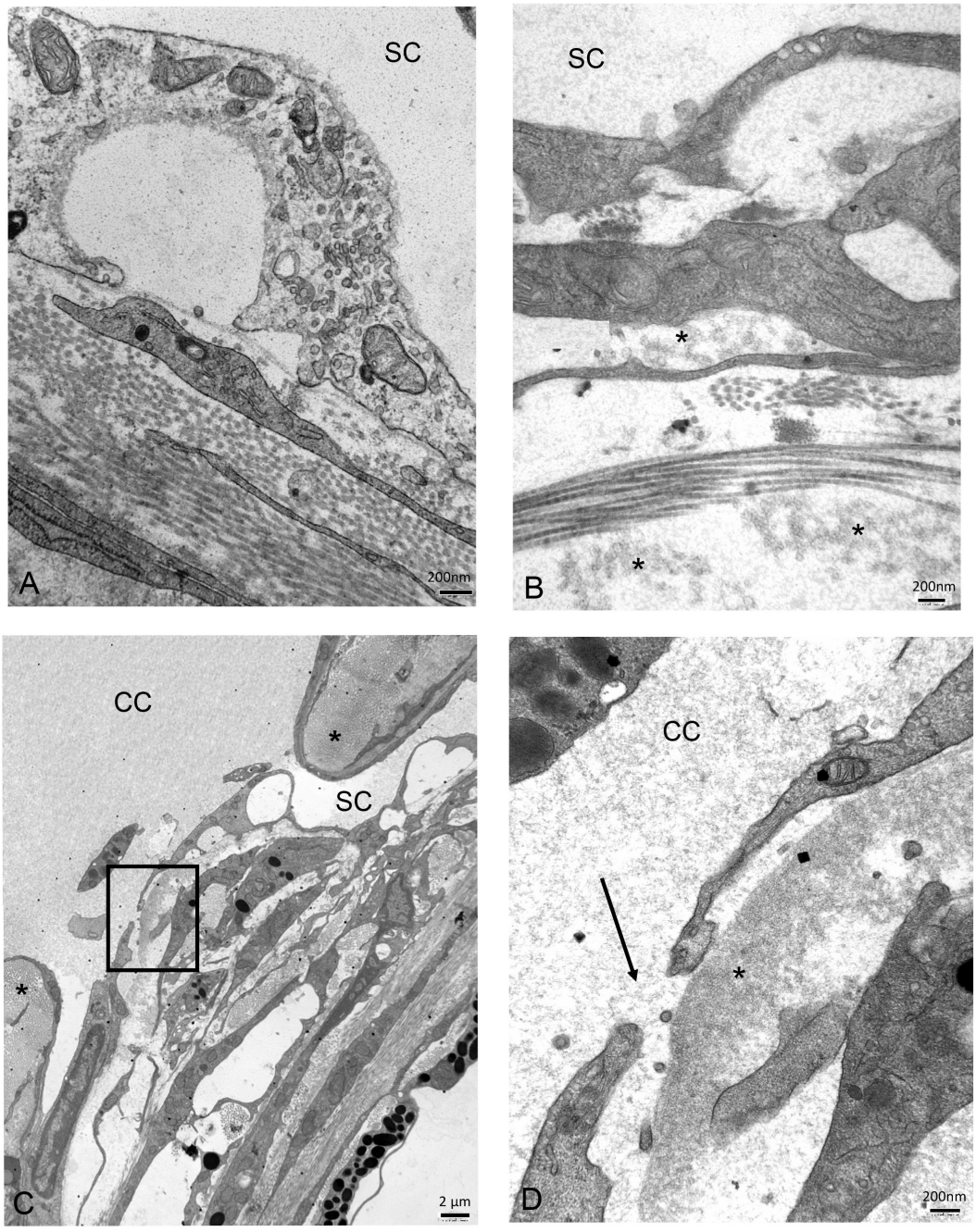

Figure 11. (A) Representative image of low-tracer region. No microbeads could be identified in the JCT region. Schlemm's canal (SC) labeled. (B) Representative image of high-tracer region. Microbeads (*) are identified within the JCT. (C) High-tracer region near collector channel (CC) ostia. The JCT near the entrance to CC ostia (*) in high-tracer regions appears less compact. The region encased in the black box is magnified in the next panel. (D) Collections of microbeads (*) were found in the open spaces of the JCT underneath a pore (arrow) amongst inner wall endothelial cells. Collector canal (CC) labeled.

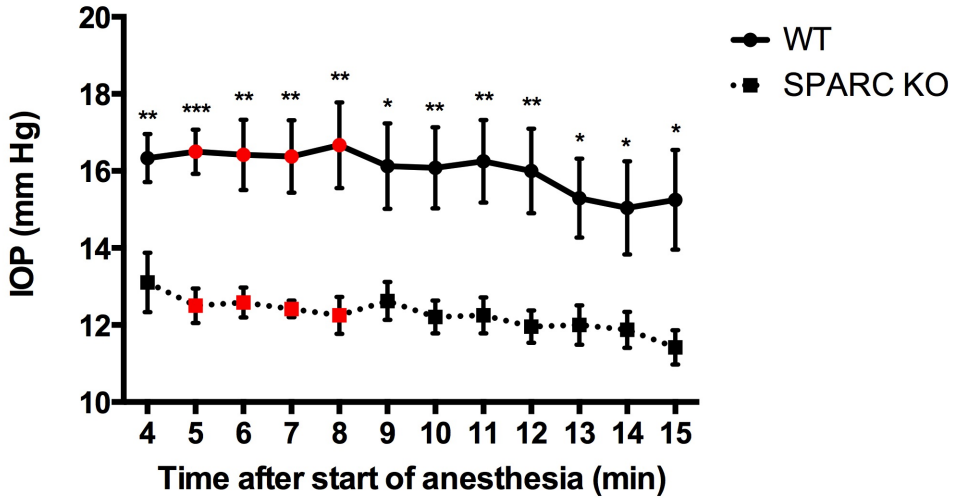

Figure 12. IOP measurements under isoflurane. IOP is relatively stable after the fifth minute. The difference in IOP between WT (N=8 animals) and KO (N=8 animals) is statistically significant at all times. All IOPs in further experiments were measured between minutes 5 and 8 (red). Data is presented as mean ± SEM. *p<0.05, **p<0.01, ***p<0.001.

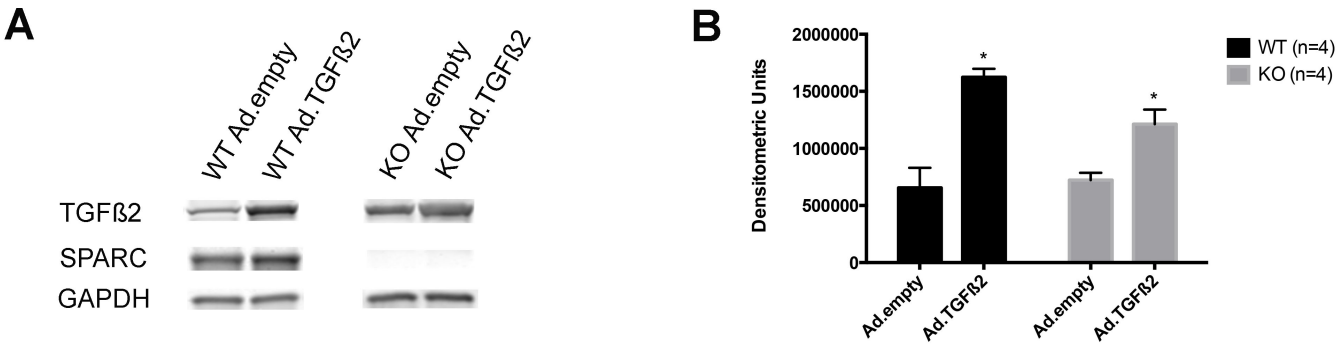

Figure 13. Immunoblot analysis for TGFß2 and SPARC in anterior segment tissue. (A) Representative immunoblot bands demonstrating a significant increase in TGFß2 with Ad.TGFß2 infection in both WT and KO tissue. SPARC was also significantly increased by approximately 56% with Ad.TGFß2 infection. (B) Densitometric quantification of immunoblot bands for TGFß2 (N=4). TGFß2 was significantly increased in WT tissue (p=0.0023) and KO tissue (p=0.0141).

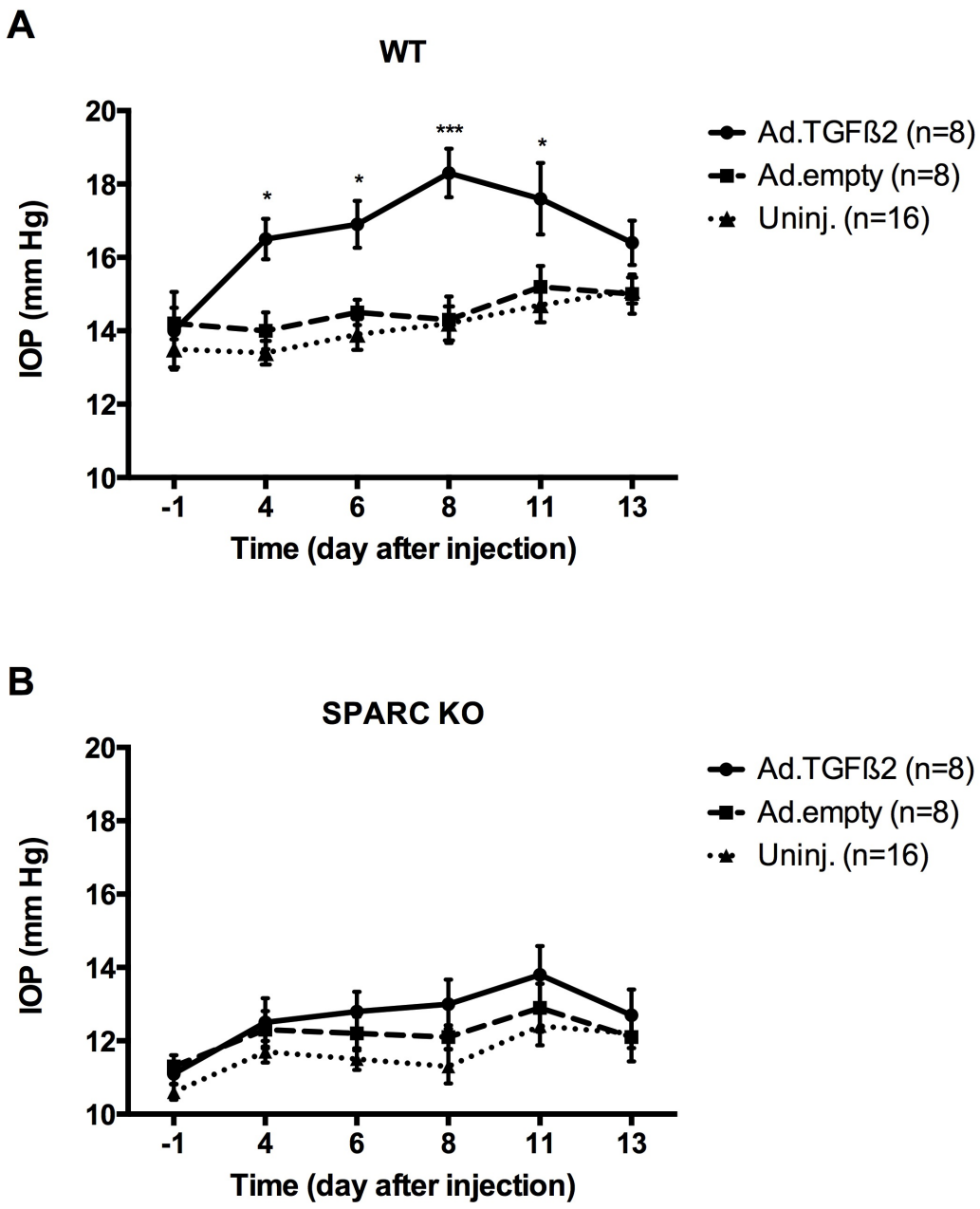

Figure 14. (A) Effects of Ad.TGFß2 injection on WT mice. IOPs of uninjected mice and mice injected with Ad.empty are also shown. The contralateral eye in the two treatment groups served as uninjected controls ("uninj."). When compared to the IOPs of Ad.empty-injected WT mice, the IOP increase of Ad.TGFß2-injected WT mice is significant during days 4-11. (B) Effects of Ad.TGFß2 injection on KO mice. Compared to the IOPs of Ad.empty-injected KO mice, the IOP increase of Ad.TGFß2-injected KO mice is not statistically significant at any time point. Data is presented as mean ± SEM. *$p<0.05$, ***$p<0.001$.

Table 1. P-values from two-way ANOVA with Bonferroni correction between the three treatment groups in WT and KO mice.

Day	-1	4	6	8	11	13
WT						
Ad.TGFß2 vs. Ad.empty	>0.9999	**0.0166**	**0.0230**	**<0.0001**	**0.0230**	0.3522
Ad.TGFß2 vs. uninj.	>0.9999	**0.0003**	**0.0004**	**<0.0001**	**0.0007**	0.2800
Ad.empty vs. uninj.	>0.9999	>0.9999	>0.9999	>0.9999	>0.9999	>0.9999
KO						
Ad.TGFß2 vs. Ad.empty	>0.9999	>0.9999	>0.9999	0.7518	0.7517	>0.9999
Ad.TGFß2 vs. uninj.	>0.9999	0.7150	0.1684	**0.0385**	0.1196	>0.9999
Ad.empty vs. uninj.	0.9059	>0.9999	0.9059	0.7150	>0.9999	>0.9999

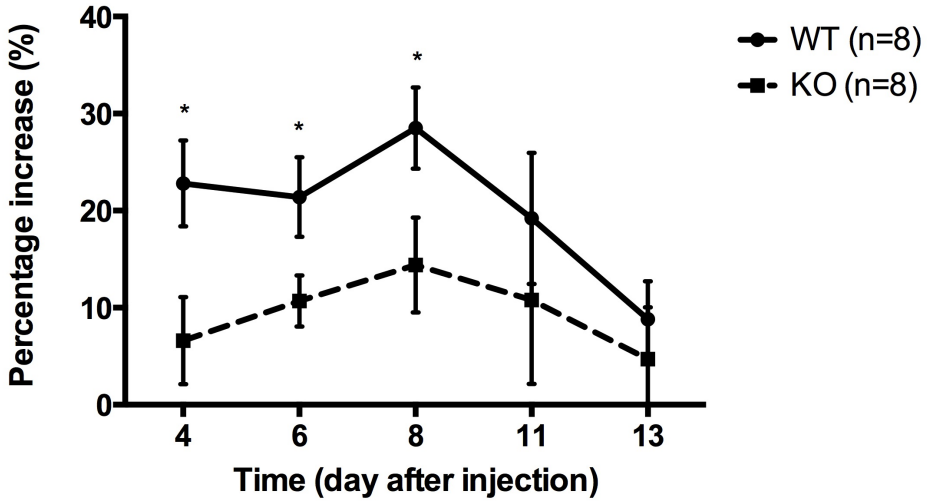

Figure 15. Comparison of percentage increase in IOP of WT and KO mice injected with Ad.TGFß2 (N=8). The difference was statistically significant at Days 4, 6, and 8. Data is presented as mean ± SEM. *p<0.05.

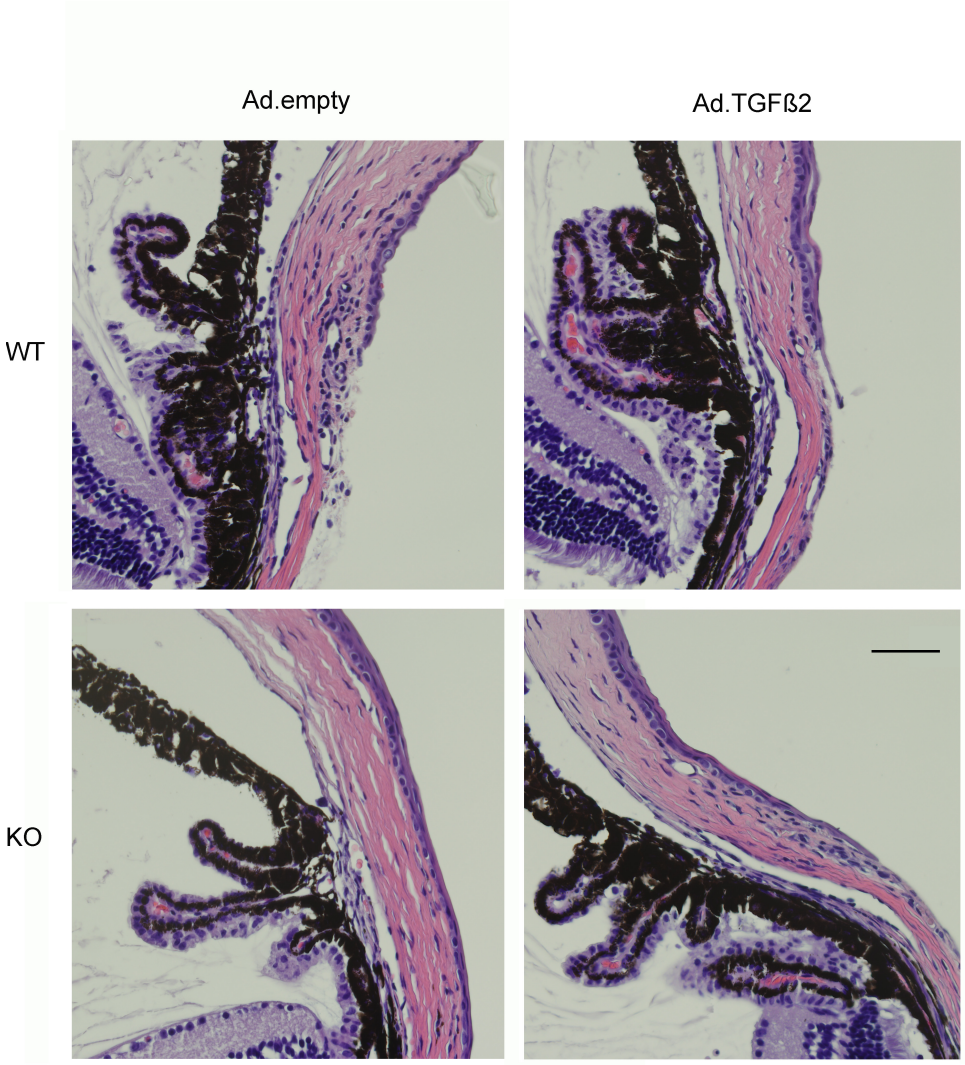

Figure 16. Representative iridocorneal angle morphology of WT and KO mice 8 days after injection with either Ad.empty or Ad.TGFß2. The iridocorneal angle remained open in all 4 groups. Scale bar, 50 µm.

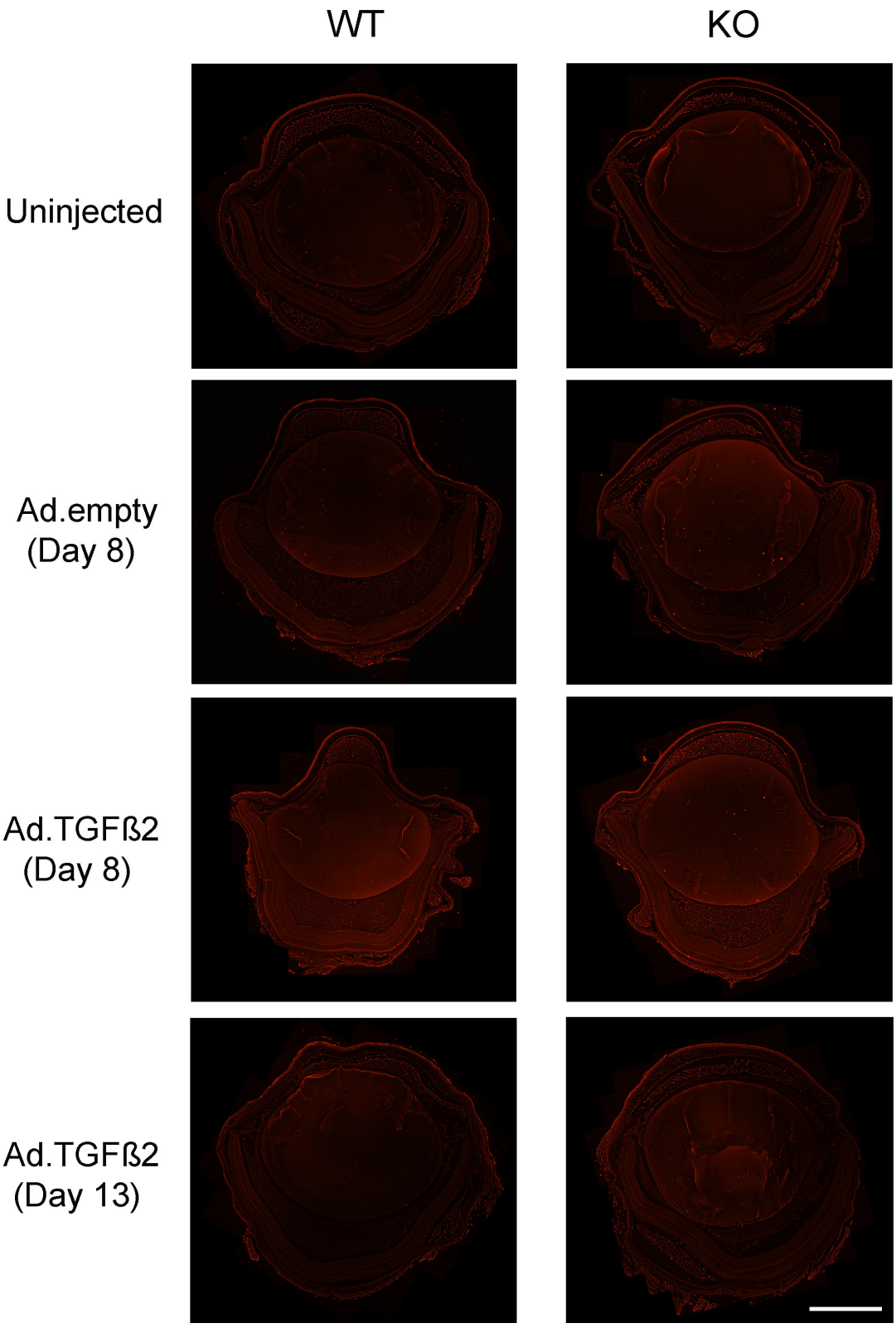

Figure 17. Sagittal sections of representative WT and KO tissue stained for TGFß2. In both WT and KO mice, Ad.empty-injected eyes had a similar staining pattern to uninjected eyes. Ad.TGFß2-injected eyes demonstrated a marked increase in staining at Day 8 within the retina, vitreous humor, and trabecular meshwork. However, this effect was nullified at Day 13. Scale bar, 800 µm.

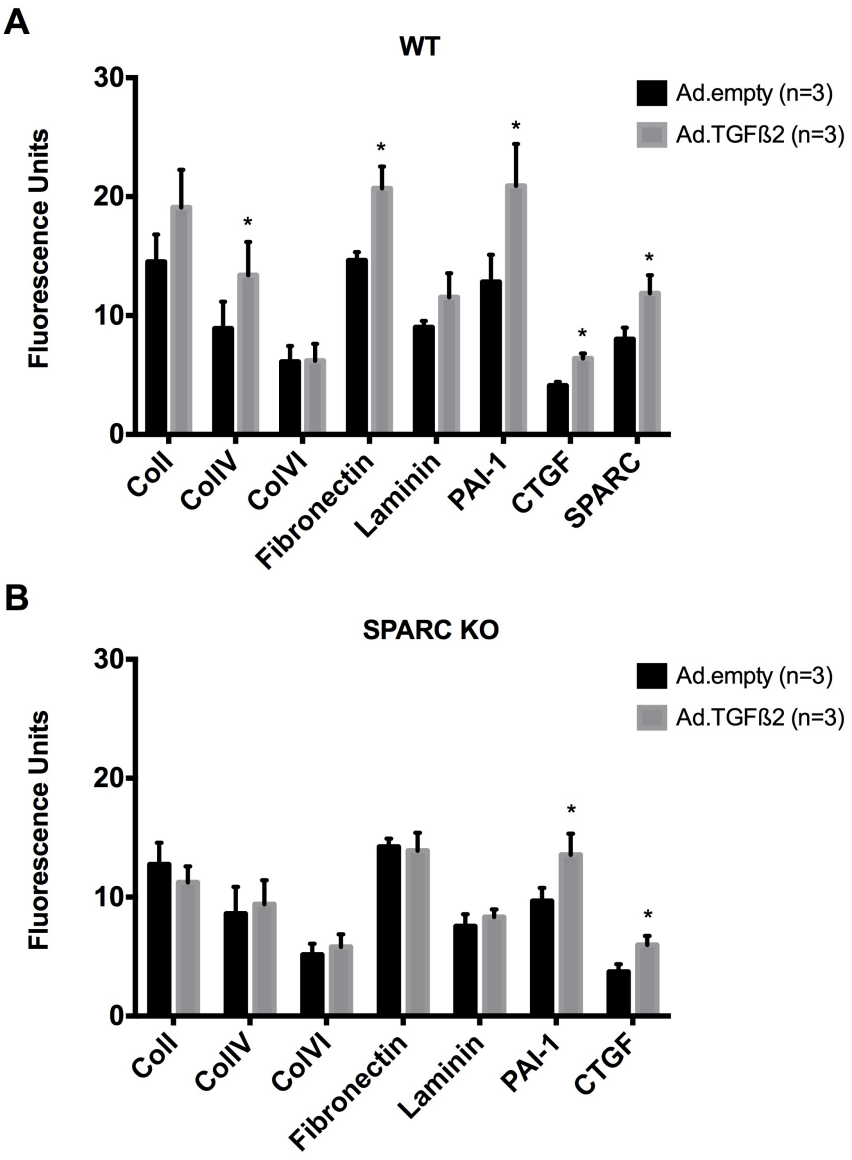

Figure 18. Changes in fluorescence intensity of select ECM proteins in (A) WT mice (B) KO mice 8 days after treatment with Ad.empty or Ad.TGFß2 (N=3). In WT tissue, the intensities of collagen IV, fibronectin, PAI-1, CTGF, and SPARC were significantly increased following TGFß2 stimulation (asterisks, $p<0.05$). In KO tissue, only PAI-1 and CTGF fluorescence increase were significant with TGFß2 stimulation (asterisks, $p<0.05$). Changes in collagen IV and fibronectin levels were non-significant. SPARC was not found in SPARC KO mice (B).

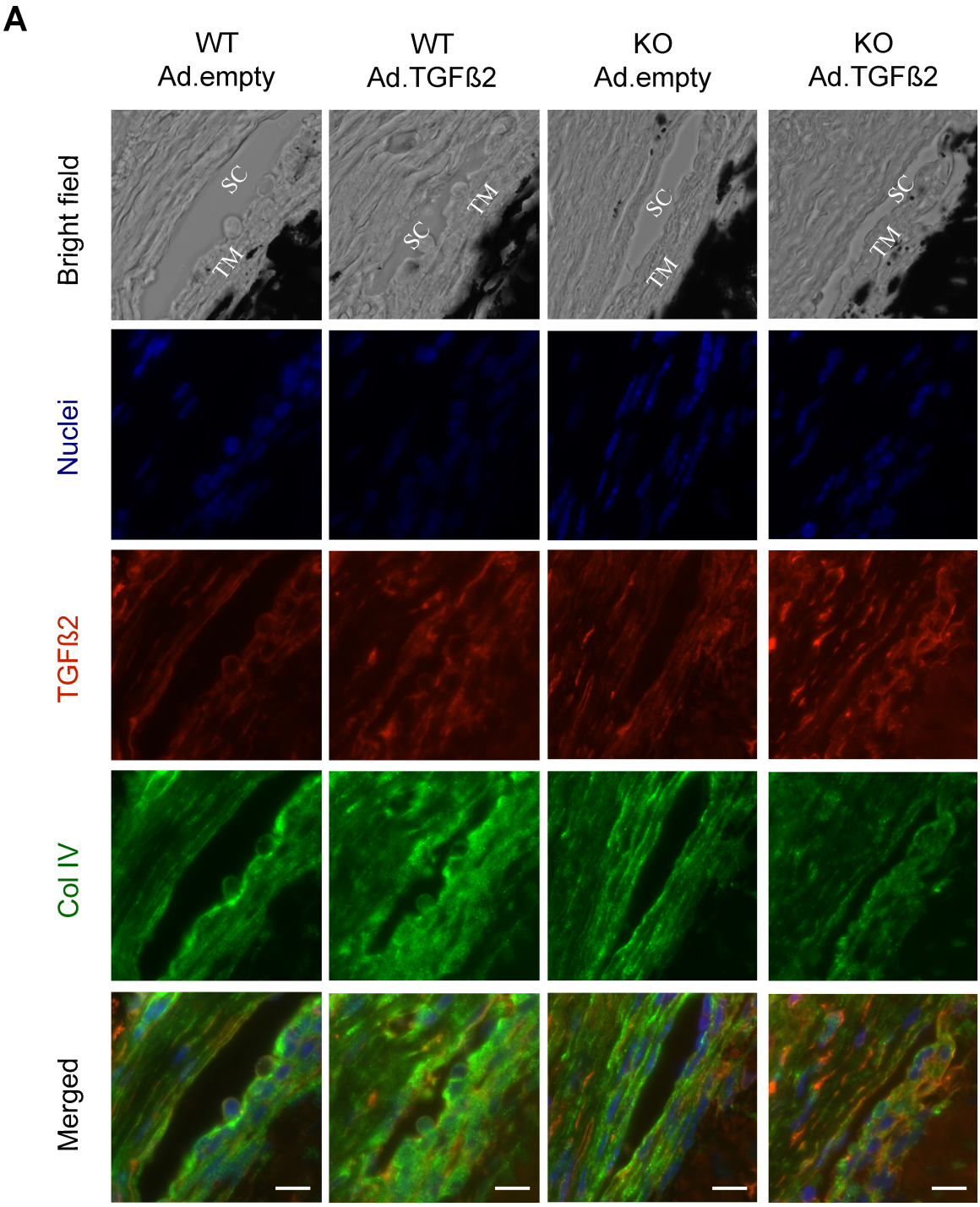
A
WT
Ad.empty
WT
Ad.TGFß2
KO
Ad.empty
KO
Ad.TGFß2
Bright field
Nuclei
TGFß2
Col IV
Merged
SC
TM

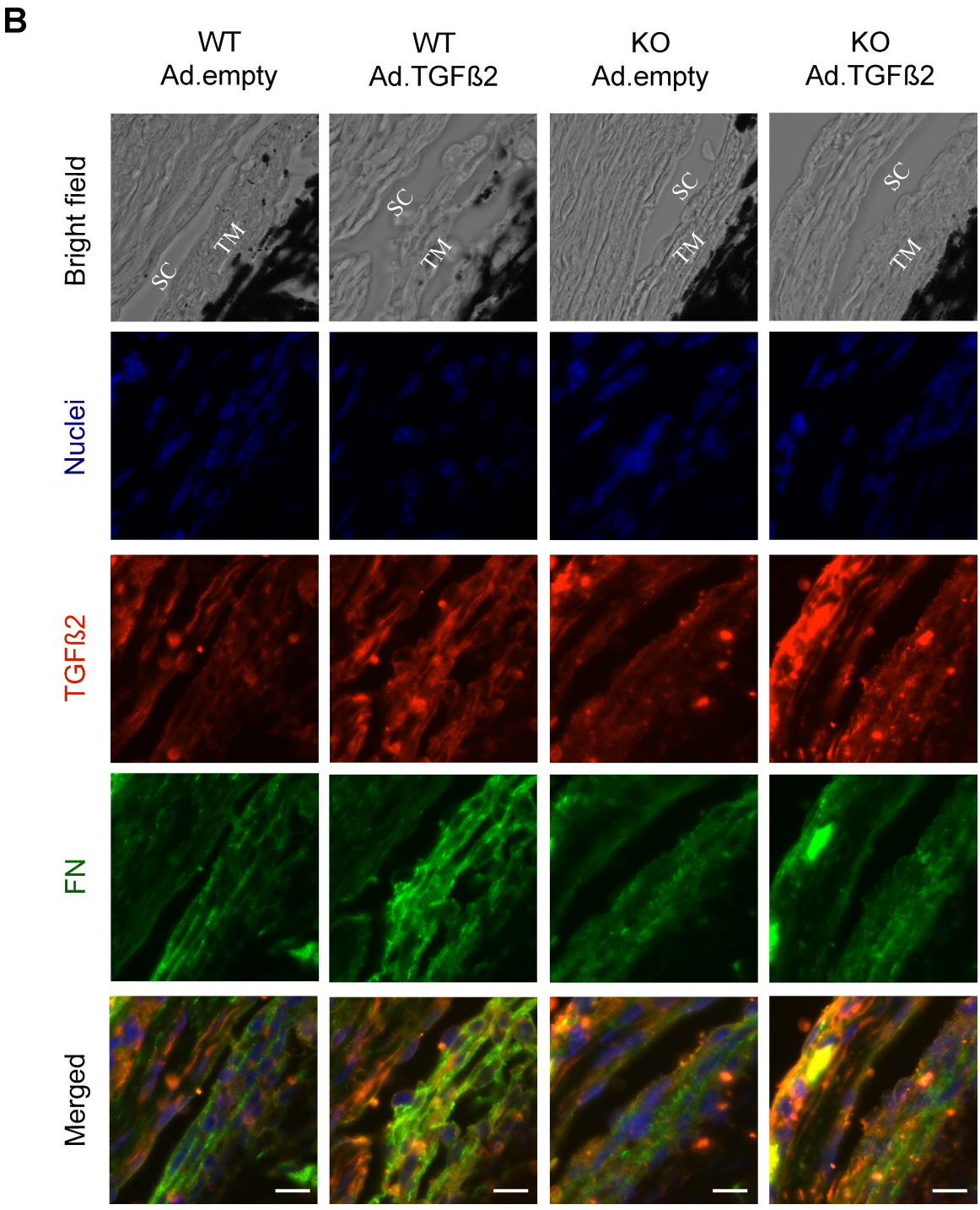
B
WT
Ad.empty
WT
Ad.TGFß2
KO
Ad.empty
KO
Ad.TGFß2
Bright field
Nuclei
TGFß2
FN
Merged
SC
TM

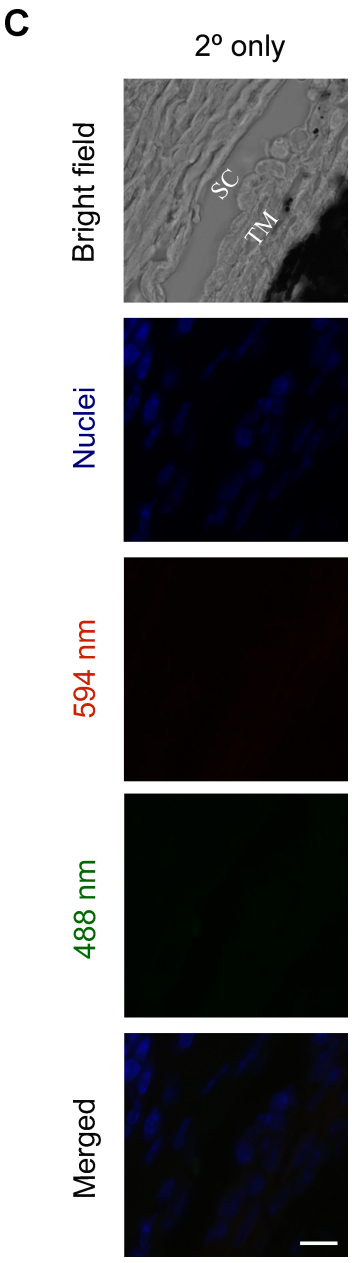

Figure 19. Representative immunolabeling of (A) collagen IV and (B) fibronectin in WT and KO mice 8 days after treatment with Ad.empty or Ad.TGFß2. Both collagen IV and fibronectin were significantly increased in Ad.TGFß2-injected WT mice, but not in Ad.TGFß2-injected KO mice compared to respective Ad.empty groups. Mild fluorescence appeared in the TGFß2 panel of the Ad.empty-injected tissue, as the primary antibody was bound to endogenous mouse TGFß2. (C) Secondary antibody-only staining is shown as a negative control. Scale bar, 10µm.

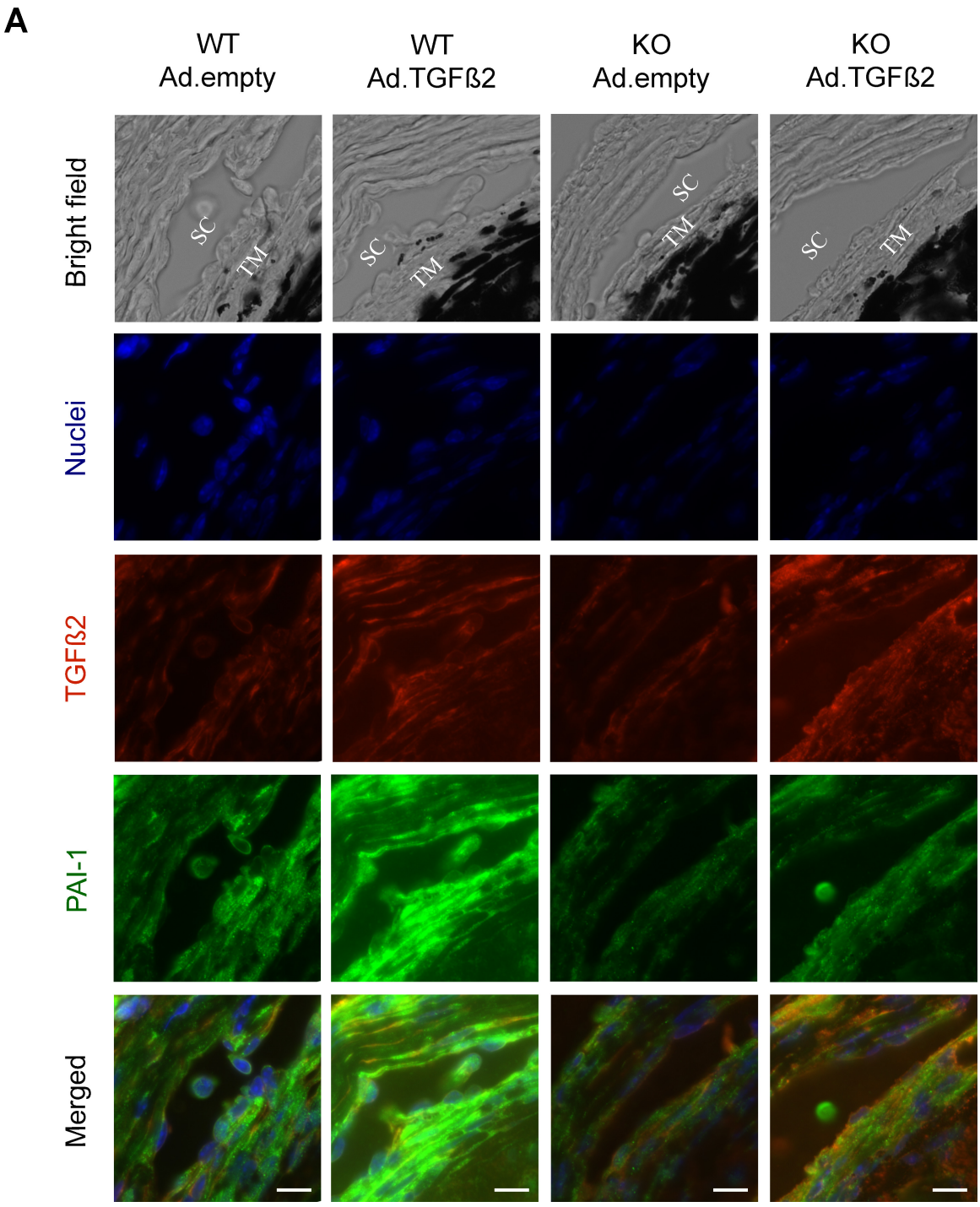
A
WT
Ad.empty
WT
Ad.TGFß2
KO
Ad.empty
KO
Ad.TGFß2
Bright field
Nuclei
TGFß2
PAI-1
Merged
SC
TM

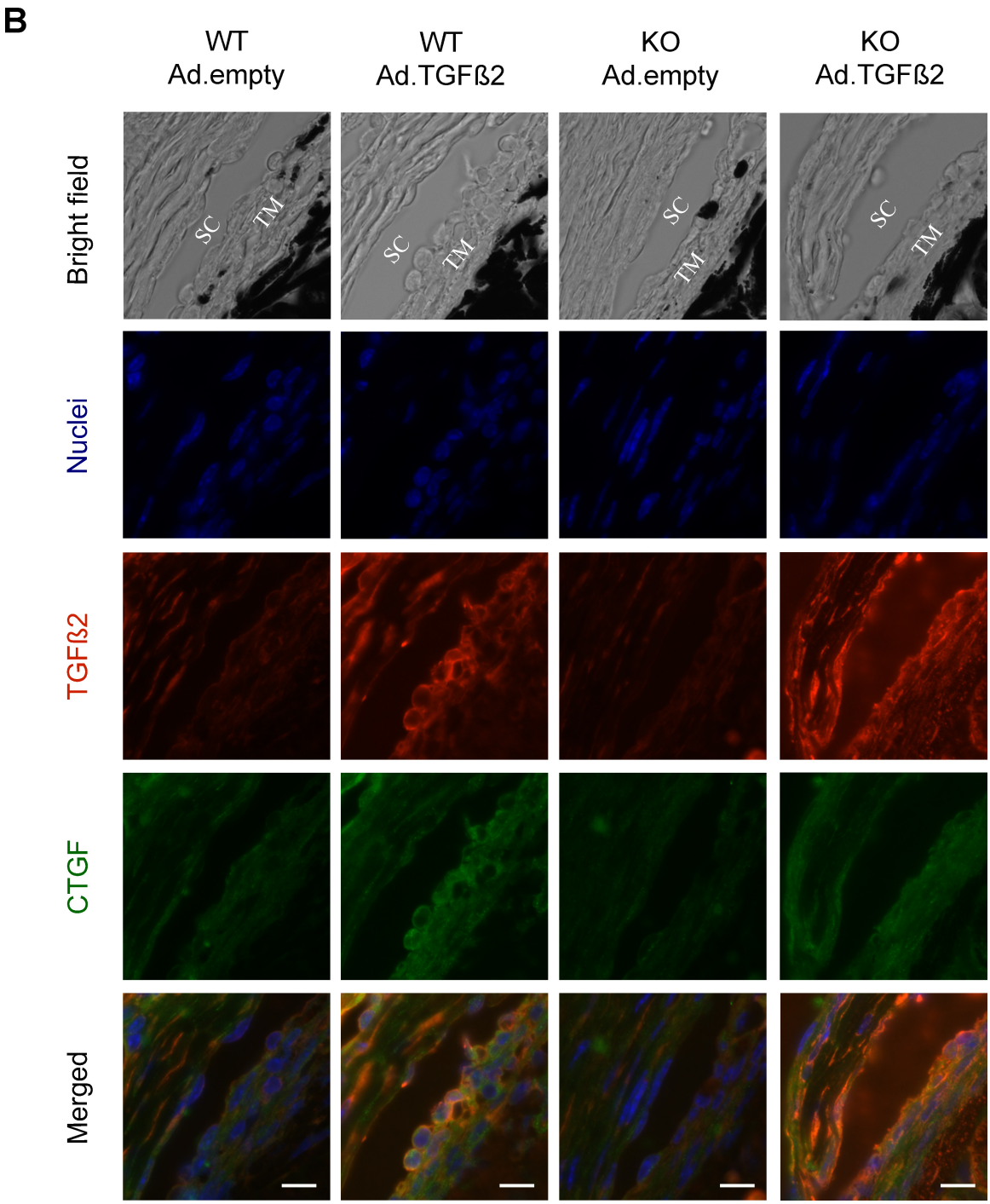
B
WT
Ad.empty
WT
Ad.TGFß2
KO
Ad.empty
KO
Ad.TGFß2
Bright field
Nuclei
TGFß2
CTGF
Merged
SC
TM

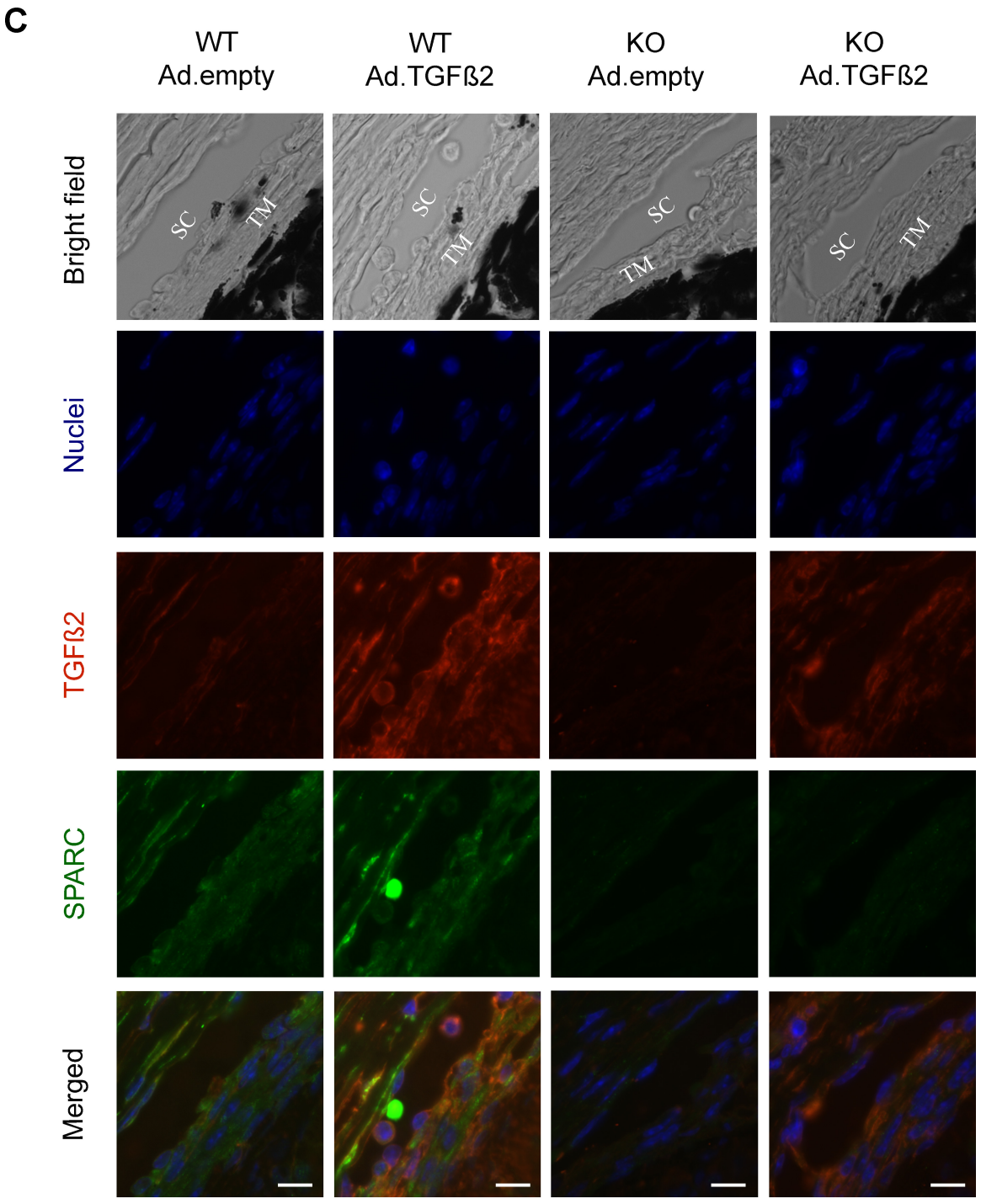
C
WT
Ad.empty
WT
Ad.TGFß2
KO
Ad.empty
KO
Ad.TGFß2
Bright field
Nuclei
TGFß2
SPARC
Merged
SC
TM

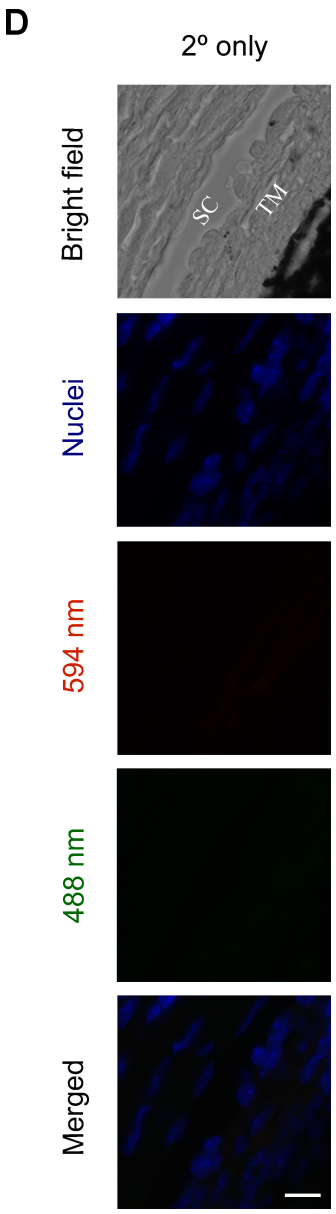

Figure 20. Representative immunolabeling of (A) PAI-1, (B) CTGF, and (C) SPARC in WT and KO mice 8 days after treatment with Ad.empty or Ad.TGFß2. PAI-1 and CTGF were significantly increased in both Ad.TGFß2-injected WT mice and Ad.TGFß2-injected KO mice compared to respective Ad.empty groups. SPARC was upregulated in Ad.TGFß2-injected WT mice, and was absent in KO mice as expected. The fluorescent artifact in the SPARC panel of Ad.TGFß2 WT was not included in calculations, as it lies outside the TM. Mild fluorescence appeared in the TGFß2 panel of the Ad.empty-injected tissue, as the primary antibody was bound to endogenous mouse TGFß2. (D) Secondary antibody-only staining is shown as a negative control. Scale bar, 10µm.

Table 2. Fluorescence intensity measurements of ECM proteins and TGFß2 from immunostained images. P-values were derived from comparing the percentage increase in WT and KO tissues using paired Student's t-tests.

ECM Protein	WT change (%)	KO change (%)	p-value
Collagen I	32.07 ± 13.57	-11.12 ± 2.91	0.0965
Collagen IV	55.13 ± 9.50	14.77 ± 12.17	**0.0227**
Collagen VI	0.95 ± 1.34	13.23 ± 13.40	0.4605
Laminin	26.38 ± 14.94	13.57 ± 15.92	0.4233
Fibronectin	40.93 ± 6.54	-2.37 ± 9.31	**0.0190**
PAI-1	64.64 ± 10.54	39.87 ± 6.42	0.2720
CTGF	57.36 ± 14.41	64.75 ± 17.28	0.7040
SPARC	48.64 ± 9.71	0	**<0.001**
TGFß2	108.74 ± 12.16	78.38 ± 22.71	0.2582